LAMINAR-FLOW HEAT TRANSFER AND PRESSURE DROP IN TUBES WITH LIQUID SOLIDIFICATION

A THESIS

Presented to

the Faculty of the Graduate Division

by

Ronald D. Zerkle

In Partial Fulfillment

of the Requirements for the Degree

Doctor of Philosophy in the School

of Mechanical Engineering

Georgia Institute of Technology

September, 1964

LAMINAR-FLOW HEAT TRANSFER AND PRESSURE DROP

IN TUBES WITH LIQUID SOLIDIFICATION

Approved:

Date approved by Chairman: September 2, 1964

ACKNOWLEDGMENTS

The author wishes to express sincere gratitude to Dr. J. E. Sunderland for his guidance and encouragement in the preparation of this thesis, and for his inspiring example as a teacher and friend.

The author wishes to acknowledge the assistance of Messrs. L. A. Cavalli, C. R. Bannister, J. G. Doyal, and L. W. Gleason in constructing various equipment for this investigation, and the financial support of the Georgia Institute of Technology and the Ford Foundation during his doctoral program.

In addition, the author wishes to thank his family for their patience and encouragement.

TABLE OF CONTENTS

TABLE OF CONTENTS (Continued)

LIST OF ILLUSTRATIONS

LIST OF ILLUSTRATIONS (Continued)

LIST OF TABLES

SUMMARY

The effect of liquid solidification at the inner surface of a circular tube upon laminar-flow heat transfer and pressure drop is investigated analytically and experimentally for steady-state conditions. The liquid flowing through the tube is assumed to be Newtonian and incompressible, and physical properties are assumed to be independent of temperature for any given phase. The liquid is isothermal and has a fully-developed velocity profile at the thermal entrance; i.e., the tube section where cooling begins. Following this section the wall temperature is constant and lower than the liquid freezing temperature. A solid-phase shell is thus formed which constricts the liquid flow and produces a two-dimensional velocity profile.

Theoretical expressions for the bulk temperature distribution, heat transfer rate, radius of the liquid-solid interface, and axial pressure distribution are determined from a mathematical analysis of the continuity, momentum, and energy equations. The mathematical analysis neglects axial heat conduction, viscous energy dissipation, radiant heat transfer, and body forces. It also assumes that the fluid flow remains laminar and the axial component of the fluid velocity retains its parabolic profile throughout the cooling region. The solution to the resulting form of the energy equation is obtained through use of a variable transformation, which transforms it to the classical Graetz equation for which the solution is known. The axial pressure distribution is determined by solving an approximate integral form of the axial momentum equation.

The experimental analysis is divided into two parts, the visual experiment and the circular tube experiment. The purpose of the visual experiment is to observe the solidification of a liquid flowing through a closed conduit. Visual observations of the solidification of water flowing through a horizontal, rectangular conduit with plexiglass top and bottom and copper side walls substantiate basic assumptions concerning the characteristics and appearance of the solid-phase shell.

The purpose of the circular tube experiment is to measure variables which enable a comparison to be made between the experimental and theoretical results. A comparison between the theoretical results and experimental data taken from two horizontal test sections of different length shows that natural convection within the liquid can produce a considerable variance in results.

A semi-empirical method for obtaining approximate solutions is also presented along with an illustrative example, which demonstrates how natural convection affects the solid-phase shell profile. This method can be used for either laminar or turbulent flow, and for fluids other than Newtonian liquids.

LIST OF SYMBOLS

c_p	Specific heat at constant pressure, B/lbm-°F
C_n	Constants occurring in the Graetz solution
D	Inside tube diameter, ft
g	Gravitational acceleration, ft/sec^2
Gr	Grashof Number, $gD^3 \beta \left[(T_o + T_b)/2 - T_w\right] / \nu^2$, dimensionless
h_{am}	Arithmetic mean heat transfer coefficient, equations (75) or (81), B/hr-ft^2-°F
I	Dimensionless integral, equation (60)
k	Thermal conductivity, B/hr-ft-°F
k_L	Thermal conductivity of the liquid
k_s	Thermal conductivity of the solid phase
L	Test section length
$\dot{m}$	Mass flowrate, lbm/min
n	Indicial notation, n = 0, 1, 2, ...
$(Nu)_{am}$	Arithmetic mean Nusselt Number, equation (77)
p	Pressure, in. H_2O
p_o	Pressure at z = 0
p^*	Dimensionless pressure drop, equation (56)
Pr	Prandtl Number, ν/a, dimensionless
q	Heat transfer rate, B/hr
q^*	Dimensionless heat transfer, equation (42) or (62)
r	Space coordinate normal to tube axis, ft
r^*	Dimensionless radial coordinate, equation (25)

LIST OF SYMBOLS (Continued)

R	Inside tube radius, ft
Re_D	Reynolds Number, VD/ν , dimensionless
R_n	Eigenfunctions occurring in the Graetz solution
R_n'	Derivative of eigenfunction occurring in the Graetz solution
T	Temperature, ^oC or ^oF
T^*	Dimensionless temperature, equation (23)
T_b	Liquid bulk temperature, equation (45)
T_b^*	Dimensionless bulk temperature, equation (47) or (61)
T_f	Freezing temperature of the liquid
T_L	Temperature of the liquid
T_o	Temperature of the liquid at $z = 0$
T_s	Temperature of the solid phase
T_w	Tube wall-temperature
T_w^*	Dimensionless parameter, equation (53)
v_r	Component of velocity in the r direction, ft/sec
v_z	Component of velocity in the z direction, ft/sec
V	Average fluid velocity at $z = 0$, ft/sec
z	Space coordinate along tube axis, ft
z^*	Dimensionless axial position, equation (24)
α	Thermal diffusivity, $k/\rho\ c_p$, ft^2/sec
β	Coefficient of volumetric expansion, $1/^oC$
δ	Radius of the liquid-solid interface, ft
δ^*	Dimensionless radius of the liquid-solid interface, equation (26)

LIST OF SYMBOLS (Continued)

η	Dimensionless radial coordinate, equation (30)
λ_n	Eigenvalues occurring in the Graetz solution
μ	Dynamic viscosity, lbm/hr-ft
μ_a	Dynamic viscosity evaluated at $(T_o + T_b)/2$
μ_w	Dynamic viscosity evaluated at T_w
ν	Kinematic viscosity, ft^2/sec
ρ	Density, lbm/ft^3

Other symbols or subscripts that might be used are defined in the text.

CHAPTER I

INTRODUCTION

The process of solidification or freezing of materials has considerable importance in many technical fields. For example, the freezing phenomenon must be confronted in the making of ice, freezing of foods, and casting of metals. But the freezing of materials does not always meet with approval. Frost formation on refrigeration cooling coils, ice formation in water mains, and solidification of molten metals and salts in nuclear-reactor heat exchangers, for example, are all detrimental to the transfer of heat and mass. Also, in the design of space satellites and other space vehicles, consideration must be given to the possibility of undesirable phase changes occurring in hydraulic systems and heat exchangers which may be subjected to extreme environmental temperatures.

Since the solidification of materials flowing in closed conduits is of such practical importance, the purpose of this investigation is to study the effects of a liquid-solid change of phase upon laminar-flow heat transfer and pressure drop in circular tubes.

Review of the Literature

Many investigations of laminar forced-convection heat transfer in conduits without solidification are presently available in the literature. The solution of the original Graetz problem of forced convection heat transfer with laminar, fully-developed flow of a constant-property

fluid through an isothermal circular tube is reviewed by Jacob (1). The Graetz problem has been extended by many authors and in a variety of ways. The most significant of these are as follows: Kays (2) considers hydrodynamically developing fluid flow; Schneider (3) and Singh (4) study the effect of axial heat conduction; Sellers, et al. (5) and Schenk and Dumore (6) consider various thermal boundary conditions; Brinkman (7) investigates the effect of viscous dissipation; Deissler (8) and Yang (9) consider variable fluid properties; and Sparrow and Siegel (10) study the transient heating problem. The corresponding problem of fluid flow between flat parallel plates has also been thoroughly studied.

A presence of natural convection within the fluid is a main source of disagreement between the analytical solution of Graetz and experimental results. Due to a resultant complication of hydrodynamic flow patterns, most studies of combined natural and forced convection in horizontal circular tubes have been empirical or semi-empirical in nature. Discussions of the Graetz solution and empirical correlations are presented by McAdams (11) and Knudsen and Katz (12). Recent contributions to the literature have been made by Jackson, et al. (13) and Oliver (14).

The existing literature concerning the solidification of materials can be conveniently separated into the following two categories:

1. Solidification of a material which is stationary relative to the heat sink.
2. Solidification of a material which is in motion relative to the heat sink.

Carslaw and Jaeger (15) review problems of the first category, which involve a one-dimensional solidification front, and Poots (16) investigates the case of a two-dimensional solidification front.

Problems of the second category are studied by Tkachev (17), Horvay (18), Bueckner and Horvay (19), and Whitehurst (20), where the heat sink is a flat plate. Tkachev investigates the flow of a viscous fluid around a plate during freezing of the fluid onto the plate. The rate of freezing is assumed to be constant over the length of the plate. Solutions are obtained for both laminar forced convection and laminar free convection through use of approximate integral forms of the Navier-Stokes and energy equations. Horvay solves the one-dimensional problem of freezing of a growing liquid column onto a flat plate through use of an electrical circuit analogy. Bueckner and Horvay investigate the freezing of an inviscid fluid onto a moving flat plate under the assumption of a constant rate of freezing along the solidification front. Whitehurst presents a theoretical and experimental investigation of frost formation from humid air to a metal plate during laminar free convection.

Studies of fluid flow in conduits with internal solidification are made by Brush (21), Chen and Rohsenow (22), Hirschberg (23), and Veynik (24).

Brush discusses the principles governing the freezing of water in mains. He divides ice into three kinds, based upon the manner in which it forms; i.e., surface ice, frazil ice, and anchor ice. Surface ice is formed by heat conduction from water to a heat sink. Frazil ice is the form which appears in running water when the temperature of the water falls below the freezing temperature, and where an ice sheet cannot form due to the agitation of the water. Anchor ice is found attached to the bottom of a river or stream. It results, according to Brush,

from the cooling of the bottom by radiation, and the resultant freezing of the water which comes into contact with the surfaces, which have been cooled below the freezing temperature.

Brush states that the formation of ice in water mains is dependent upon the temperature of the water and the flow rate. If the wall temperature is reduced below the freezing temperature, a coating of surface ice is formed on the inside of the pipe. If the flow rate is reduced through an increased pressure drop, the water in the main is more readily cooled, and the ice coating increases in thickness. It is probable that where the flow rate is high, the water is cooled slightly below the freezing temperature and frazil ice is formed which eventually clogs the main, stopping the flow and the whole mass of water in the main freezes. Brush states further that freezing of water mains, which lie above the frost line, can be prevented only by having such a mass flow rate that the extent of heat removal is not sufficient to cause the water temperature to fall below the freezing temperature. No analytical or experimental observations are presented by Brush.

Chen and Rohsenow present a combined experimental and theoretical study of the heat, mass, and momentum transfer inside tubes in which the condensable component of a gas mixture is removed from the stream by causing it to solidify as a frost on the tube inner surface. The transient formation of frost from a turbulent gas stream is considered. The authors show that the surface roughness of the frost is the single most important factor in the determination of heat transfer and pressure drop. Their theoretical predictions are in only fair agreement with experimental results due to the assumptions utilized to solve this

extremely complicated problem, and to the fact that the physical properties of frost vary greatly with the rate of formation.

Hirschberg analyzes the complete freezing of pipes through which a liquid flows. By assuming laminar flow, constant inlet pressure, constant heat transfer coefficient between the liquid and the ice layer, resistance to flow inversely proportional to the decreasing mass flow rate, and solid-phase shell thickness uniform throughout the cooling length, a relation is determined between the parameters for complete freezing of pipes. Hirschberg presents no experimental verification of his theoretical results, but experimentally determined freezing times for various stagnant liquid solutions in pipes and the pressure resistance of these plugs are presented.

Veynik analyzes the continuous casting of metals. The continuous casting process consists of pouring molten metal into a water-cooled mold, and then continually removing the solidified metal from the mold. Figure 1 shows a schematic diagram of the solidification of a continucus casting. Veynik assumes steady-state conditions, constant properties, all heat transfer coefficients constant, constant temperature of crystallization, and negligible axial heat conduction and natural convection. Also, by assuming a uniform cross-sectional temperature in zone II (based on experimental evidence) and a linear radial temperature distribution in zone III, theoretical relations are determined for z', z'', d and the temperature field in the casting for flat, cylindrical, and annular castings.

In summary, it can be stated that previous investigators have analyzed convection heat transfer in ducts without solidification, and

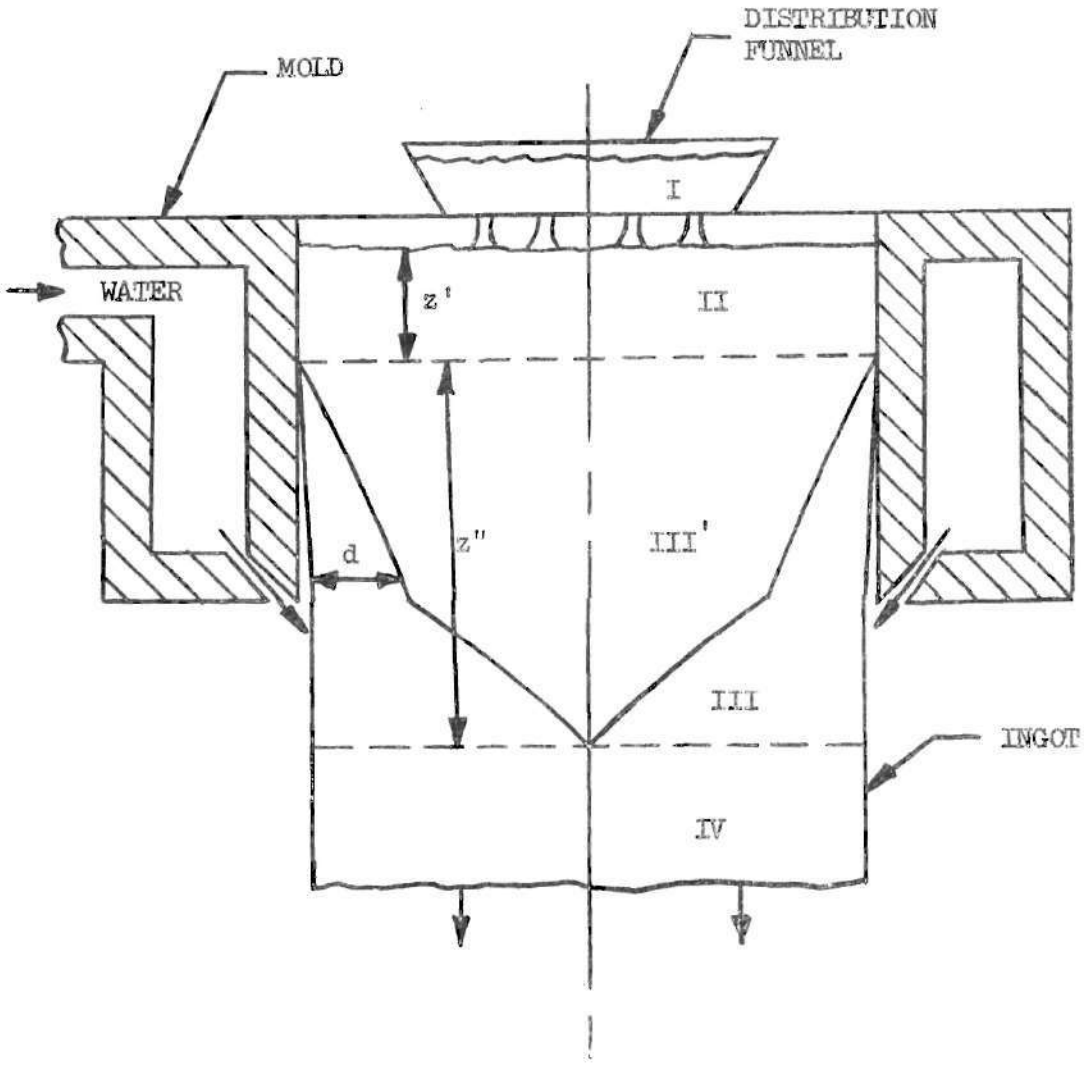

I - POURING ZONE

II - ZONE OF SUPERHEAT REMOVAL

III - SOLIDIFICATION ZONE

III' - LIQUID METAL SURROUNDED BY FROZEN CRUST

IV - ZONE OF FULLY-SOLIDIFIED METAL

Figure 1. Schematic Diagram of the Solidification of a Continuous Casting.

solidification of materials at rest relative to the heat sink. However, there is still much work to be done with regard to solidification of a material which is in motion relative to the heat sink. More specifically, there has been, to the author's knowledge, no satisfactory analysis of the effect of the solidification of a liquid flowing in a duct upon the heat transfer and pressure drop.

The object of this thesis is to present theoretical and experimental studies of the effect of a liquid-solid change of phase upon the heat transfer and pressure drop in circular tubes. The investigation is made for laminar flow and steady-state conditions.

Statement of the Problem

This investigation is concerned with finding the steady-state temperature distribution, radial thickness of the solid phase, and axial pressure distribution in a liquid flowing through a circular tube with solidification at the inner wall surface. The liquid is assumed to have a uniform temperature and a fully-developed velocity profile at the thermal entrance; i.e., the tube section where cooling begins. Following this section the wall temperature is constant and lower than the liquid freezing temperature. The liquid is cooled as it flows through the remaining tube length by convective heat transfer to the surface of the fused liquid, which has formed on the tube wall. As the liquid proceeds along the tube, its mean temperature approaches the liquid freezing temperature, and the thickness of the fused-liquid shell increases. Due to this constriction of the flow area, the fluid is accelerated, thereby producing a two-dimensional velocity profile. The physical model is shown in Figure 2.

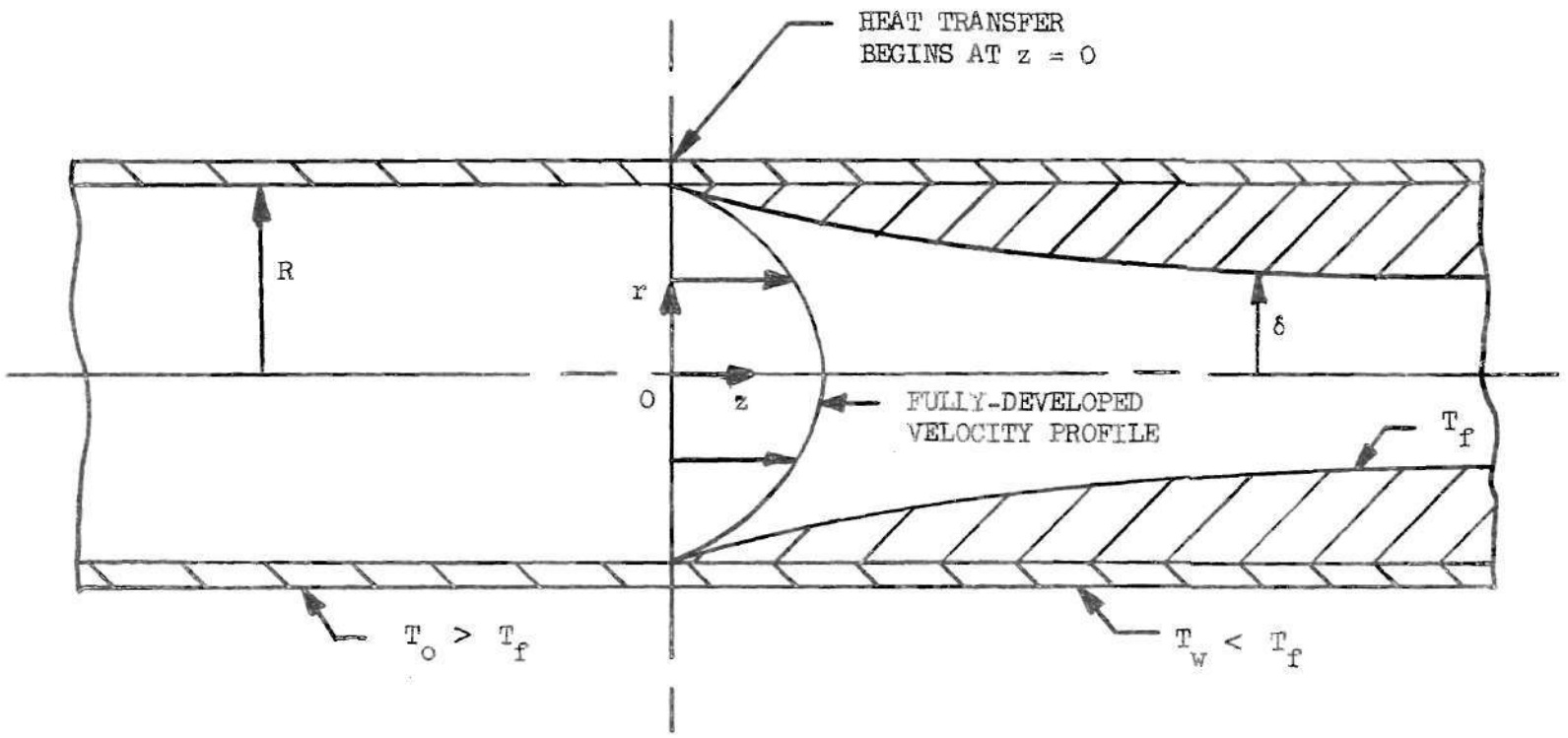

Figure 2. Sectional View at the Thermal Entrance of a Circular Tube with Solidification.

The problem is described mathematically by the conservation of mass, momentum, and energy equations along with appropriate boundary conditions. The following assumptions are made in this investigation:

1. Steady-state conditions prevail.
2. The liquid flow is everywhere laminar, and is fully-developed and isothermal at the thermal entrance.
3. The liquid is Newtonian and incompressible.
4. Physical properties of each phase are independent of temperature.
5. Axial heat conduction, viscous energy dissipation, radiant heat transfer, and body forces are negligible.
6. The liquid freezing temperature (T_f) is constant.
7. The tube wall has negligible thermal resistance, and a temperature (T_w) in the cooling region, which is constant and lower than the liquid freezing temperature.
8. The solid-phase shell is smooth, homogeneous, and isotropic, and has a monotonically increasing thickness beginning at the thermal entrance section.

After imposing the above assumptions, the continuity, momentum, and energy equations are reduced to the following forms. The continuity relation can be expressed as

$$\frac{1}{r}\frac{\partial (rv_r)}{\partial r} + \frac{\partial v_z}{\partial z} = 0 \qquad (1)$$

or

$$2\int_0^{\delta} v_z r\,dr = R^2 V \qquad (2)$$

The momentum equation for the r-direction is

$$v_r \frac{\partial v_r}{\partial r} + v_z \frac{\partial v_r}{\partial z} = - \frac{1}{\rho} \frac{\partial p}{\partial r} + \nu \left[\frac{\partial}{\partial r} \left(\frac{1}{r} \frac{\partial (r v_r)}{\partial r} \right) + \frac{\partial^2 v_r}{\partial z^2} \right] \tag{3}$$

and for the z-direction is

$$v_r \frac{\partial v_z}{\partial r} + v_z \frac{\partial v_z}{\partial z} = - \frac{1}{\rho} \frac{\partial p}{\partial z} + \nu \left[\frac{1}{r} \frac{\partial}{\partial r} \left(r \frac{\partial v_z}{\partial r} \right) + \frac{\partial^2 v_z}{\partial z^2} \right] \tag{4}$$

The boundary conditions are

$$v_r(\delta, z) = 0 \tag{5}$$

$$v_z(\delta, z) = 0 \tag{6}$$

$$v_r(0, z) = 0 \tag{7}$$

$$\frac{\partial v_z}{\partial r}(0, z) = 0 \tag{8}$$

$$v_z(r, 0) = 2V \left[1 - (r/R)^2 \right] \tag{9}$$

$$p(r, 0) = p_0 \tag{10}$$

The equation for the temperature distribution in the liquid downstream from the thermal entrance is

$$v_r \frac{\partial T}{\partial r} + v_z \frac{\partial T}{\partial z} = \alpha \left[\frac{1}{r} \frac{\partial}{\partial r} \left(r \frac{\partial T}{\partial r} \right) \right] \tag{11}$$

for which the boundary conditions are

$$T(r, 0) = T_0 \tag{12}$$

$$T(\delta,z) = T_f \tag{13}$$

The temperature in the solid-phase shell is described by the equation

$$\frac{d}{dr}\left(r\,\frac{dT}{dr}\right) = 0 \tag{14}$$

together with the boundary conditions

$$T(R,z) = T_w \tag{15}$$

$$T(\delta,z) = T_f \tag{16}$$

An additional relation necessary for the determination of $\delta(z)$ is obtained from an energy balance between the liquid and the solid-phase shell. Therefore,

$$k_L \frac{\partial T_L}{\partial r}(\delta,z) = k_s \frac{\partial T_s}{\partial r}(\delta,z) \tag{17}$$

The analytical investigation presented in Chapter II is concerned with solving the above equations subject to the prescribed boundary conditions.

CHAPTER II

MATHEMATICAL ANALYSIS

The analytical solution consists of finding the fluid velocity distribution, the temperature distribution, the radius of the liquid-solid interface $\delta(z)$, and the axial pressure distribution.

The primary problem is to determine the fluid velocity distribution through a duct with variable flow area. After the fluid velocity is determined, then the temperature distribution and $\delta(z)$ can be found. But solving the system of equations (1-17) is complicated by the fact that the momentum and energy equations are coupled by their boundary conditions, i.e., the varying flow radius $\delta(z)$. Due to this coupling, numerical or other approximate methods must be utilized to obtain a solution.

Fluid Velocity Distribution

It is assumed in this investigation that the axial component of the fluid velocity retains its parabolic profile throughout the cooling region. There are two effects which lead to this assumption. The first is that cooling of a liquid flowing in a tube tends to decrease the velocity near the wall and increase the velocity in the central region. This produces a velocity profile of the form represented by curve A in Figure 3. The effect is studied for flow in circular tubes of constant diameter by Yang (9). It depends upon the fact that the viscosity of a liquid increases with decreasing temperature. Since liquid being

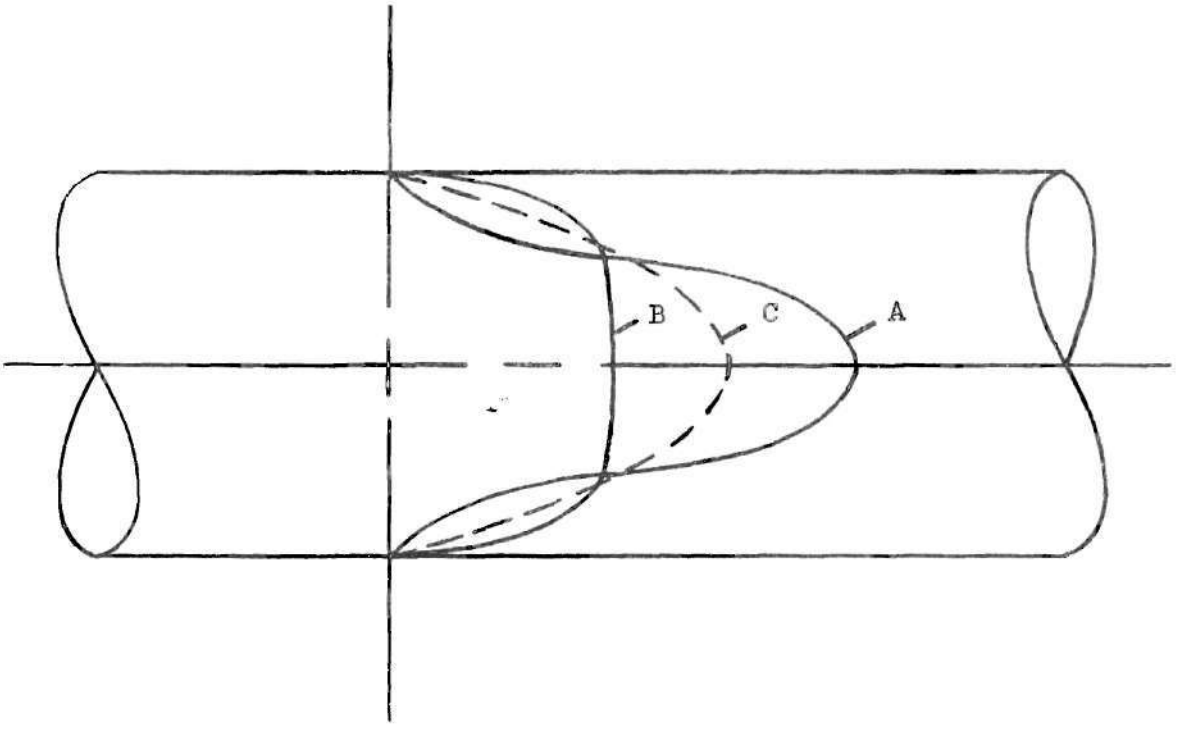

CURVE A: VELOCITY DISTRIBUTION FOR COOLING OF A LIQUID IN A TUBE WITH CONSTANT DIAMETER

B: VELOCITY DISTRIBUTION FOR ACCELERATING, ISOTHERMAL FLOW IN A TUBE WITH DECREASING DIAMETER

C: VELOCITY DISTRIBUTION FOR FULLY-DEVELOPED, ISOTHERMAL FLOW IN A TUBE WITH CONSTANT DIAMETER

Figure 3. Axial Velocity Distributions in Tubes.

cooled in a tube has a lower temperature near the wall, its viscosity is correspondingly higher there, resulting in a profile which differs from the parabolic profile occurring in isothermal flow.

The second effect is that the velocity profile of a fluid flowing through a duct with decreasing diameter is flatter than a parabolic profile. This is due to the fact that when a viscous fluid accelerates through a decreasing flow area, the increase of momentum must be transferred from the fluid near the wall to the central region. Such a profile is represented by curve B in Figure 3.

The above two effects tend to be offsetting in the case of liquid flow with solidification. For fully-developed isothermal flow in a circular tube, both effects are nonexistent and the velocity profile is parabolic. But if a difference exists between the mean liquid temperature and the wall temperature, such that solidification takes place, then both effects are introduced. It is assumed here that the combination of these effects is sufficiently negligible or that they might even cancel one another such that the velocity distribution remains parabolic. Thus, it is possible to satisfy the continuity relation and boundary conditions (5-9), but the momentum equations (3,4) will only be approximately satisfied.

It is assumed that the axial component of the liquid velocity has a quadratic form

$$v_z(r,z) = a(z) + b(z)r + c(z)r^2 \tag{18}$$

where $a(z)$, $b(z)$, and $c(z)$ are to be determined from

$$v_z(\delta,z) = 0 \tag{6}$$

$$\frac{\partial v_z}{\partial r}(0,z) = 0 \tag{8}$$

$$2\int_0^{\delta} v_z r dr = R^2 V \tag{2}$$

The quadratic coefficients satisfying relations (6), (8), and (2) are: $a(z) = 2V(R/\delta)^2$; $b(z) = 0$; and $c(z) = -2VR^2/\delta^4$. Substitution of these coefficients into equation (18) results in the following expression for the axial velocity component

$$v_z(r,z) = 2V(R/\delta)^2 \left[1 - (r/\delta)^2\right] \tag{19}$$

Equation (19) satisfies boundary condition (9), since $\delta = R$ at $z = 0$, and (19) reduces to

$$v_z(r,0) = 2V\left[1 - (r/R)^2\right] \tag{9}$$

From the continuity equation (1)

$$v_r(r,z) = -\frac{1}{r}\int_0^r r \frac{\partial v_z}{\partial z} dr \tag{20}$$

Substituting equation (19) into (20) and integrating yields for the radial velocity component

$$v_r(r,z) = 2V \frac{rR^2}{\delta^3}\frac{d\delta}{dz}\left[1 - (r/\delta)^2\right] \tag{21}$$

Equation (21) satisfies relations (5) and (7), since for $r = \delta$ and $r = 0$, (21) reduces to

$$v_r(\delta, z) = 0 \tag{5}$$

$$v_r(0, z) = 0 \tag{7}$$

Now that the fluid velocity distribution has been determined in the form of equations (19) and (21), the next step is to find the temperature distribution.

Temperature Distribution

After substituting equations (19) and (21) into equation (11), which describes the temperature in the liquid downstream from the thermal entrance, equation (11) becomes

$$2V(R/\delta)^2\left[1 - (r/\delta)^2\right]\left[\frac{r}{\delta}\frac{d\delta}{dz}\frac{\partial T}{\partial r} + \frac{\partial T}{\partial z}\right] \tag{22}$$

$$= \alpha\left[\frac{\partial^2 T}{\partial r^2} + \frac{1}{r}\frac{\partial T}{\partial r}\right], \quad (0 \leq r \leq \delta, z \geq 0)$$

for which the boundary conditions are

$$T(r, 0) = T_o \tag{12}$$

$$T(\delta, z) = T_f \tag{13}$$

Equations (22), (12), and (13) can be put into dimensionless form by making use of the following definitions:

$$T^* = (T - T_f)/(T_o - T_f) \tag{23}$$

$$z^* = 4z/D\,Re_D Pr = z\alpha/R^2 V \tag{24}$$

$$r^* = r/R \tag{25}$$

$$\delta^* = \delta / R \tag{26}$$

The quantity T^* is the dimensionless temperature, z^* is the dimensionless axial position variable, r^* is the dimensionless radial position variable, and δ^* is the dimensionless radius of the liquid-solid interface.

Substitution of the above dimensionless quantities into equations (22), (12), and (13) changes them to

$$\frac{2}{\delta^{*2}}\left[1 - (r^*/\delta^*)^2\right]\left[\frac{r^*}{\delta^*}\frac{d\delta^*}{dz^*}\frac{\partial T^*}{\partial r^*} + \frac{\partial T^*}{\partial z^*}\right] \tag{27}$$

$$= \left[\frac{\partial^2 T^*}{\partial r^{*2}} + \frac{1}{r^*}\frac{\partial T^*}{\partial r^*}\right], (0 \le r^* \le \delta^*,\ z^* \ge 0)$$

$$T^*(r^*, 0) = 1 \tag{28}$$

$$T^*(\delta^*, z^*) = 0 \tag{29}$$

This system is complicated by the appearance of the unknown δ^*. Therefore, it is proposed that a variable transformation be introduced which will at least make boundary condition (29) more tractable; i.e., define

$$\eta = r^*/\delta^* \tag{30}$$

Applying the chain rule of partial differentiation to the variable transformation of $T^*(r^*, z^*)$ to $T^*(\eta, z^*)$ gives the following relations:

$$\left[\frac{\partial T^*}{\partial r^*}\right]_{z^*} = \frac{1}{\delta^*}\left[\frac{\partial T^*}{\partial \eta}\right]_{z^*} \tag{31}$$

$$\left[\frac{\partial^2 T^*}{\partial r^{*2}}\right]_{z^*} = \frac{1}{\delta^{*2}}\left[\frac{\partial^2 T^*}{\partial \eta^2}\right]_{z^*} \tag{32}$$

$$\left[\frac{\partial T^*}{\partial z^*}\right]_{r^*} = \left[\frac{\partial T^*}{\partial z^*}\right]_{\eta} - \frac{\eta}{\delta^*}\frac{d\delta^*}{dz^*}\left[\frac{\partial T^*}{\partial \eta}\right]_{z^*} \tag{33}$$

After substitution of equations (30-33) into equations (27-29), the resulting system is

$$2(1-\eta^2)\frac{\partial T^*}{\partial z^*} = \left[\frac{\partial^2 T^*}{\partial \eta^2} + \frac{1}{\eta}\frac{\partial T^*}{\partial \eta}\right], \quad (0 \leq \eta \leq 1,\ z^* \geq 0) \tag{34}$$

$$T^*(\eta, 0) = 1 \tag{35}$$

$$T^*(1, z^*) = 0 \tag{36}$$

Not only is the unknown δ^* absent from equations (34-36), but this system, describing the dimensionless temperature distribution in the liquid, also has the same form as the system describing the Graetz problem. Thus, by means of the variable transformation (30), the system (27-29) is transformed to the system (34-36) for which the solution is known. It is

$$T^*(\eta, z^*) = \sum_{n=0}^{\infty} C_n R_n(\eta)\exp(-\lambda_n^2 z^*/2) \tag{37}$$

The temperature gradient at the liquid-solid interface is

$$\left[-\frac{\partial T^*}{\partial \eta}(1, z^*)\right] = 2\sum_{n=0}^{\infty}\left[-C_n R_n'(1)/2\right]\exp(-\lambda_n^2 z^*/2) \tag{38}$$

and the integral of the temperature gradient along the liquid-solid interface is

$$\int_0^{z^*} \left[- \frac{\partial T^*}{\partial \eta} (1,z^*) \right] dz^* = 4 \sum_{n=0}^{\infty} \left[-C_n R_n'(1)/2 \right] (\lambda_n)^{-2} \left[1 - \exp(-\lambda_n^2 z^*/2) \right] \qquad (39)$$

The quantities λ_n, C_n, R_n, and $(-C_n R_n'(1)/2)$ are given by Sellers, et al. (5) for all values of n. The quantities λ_n and $(-C_n R_n'(1)/2)$ are reproduced in Appendix A.

Heat Transfer Rate

The rate of heat transfer from the liquid for a tube of length z is

$$q = 2\pi k_L \int_0^z \left[- \delta \frac{\partial T_L}{\partial r} (\delta, z) \right] dz \qquad (40)$$

From equations (23), (25), (26), and (31)

$$\left[- \delta \frac{\partial T_L}{\partial r} (\delta, z) \right] = (T_o - T_f) \left[- \frac{\partial T^*}{\partial \eta} (1,z^*) \right] \qquad (41)$$

If the dimensionless heat transfer rate q^* is defined as

$$q^* = q/\pi R^2 V \rho c_p (T_o - T_f) \qquad (42)$$

then combining equations (40), (41), and (42) gives the following relation for the dimensionless heat transfer rate:

$$q^* = 2 \int_0^{z^*} \left[- \frac{\partial T^*}{\partial \eta} (1,z^*) \right] dz^* \qquad (43)$$

Therefore, the rate of heat transfer from the tube can be determined

analytically through use of equations (43) and (39).

Liquid Bulk Temperature

An equation for the liquid bulk temperature is derived as follows. From an energy balance applied to a tube of length z

$$\pi R^2 V \rho c_p T_o = q + \rho c_p \int_0^{\delta} T v_z 2\pi r dr \tag{44}$$

The liquid bulk temperature T_b is defined as

$$T_b = \frac{2}{R^2 V} \int_0^{\delta} T v_z r dr \tag{45}$$

Combining equations (44) and (45) and solving for T_b yields

$$T_b = T_o - q/\pi R^2 V \rho c_p \tag{46}$$

If the dimensionless bulk temperature T_b^* is defined as

$$T_b^* = (T_b - T_f)/(T_o - T_f) \tag{47}$$

then rearranging equation (46) into the form of equation (47) and substituting equation (42) gives the following relation for the dimensionless bulk temperature:

$$T_b^* = 1 - q^* \tag{48}$$

Solid-Phase Shell Profile

The radius of the liquid-solid interface $\delta(z)$ can be determined from equation (17).

$$k_L \frac{\partial T_L}{\partial r}(\delta, z) = k_s \frac{\partial T_s}{\partial r}(\delta, z) \tag{17}$$

From equation (41), the temperature gradient in the liquid at the liquid-solid interface is

$$\frac{\partial T_L}{\partial r}(\delta, z) = \frac{(T_o - T_f)}{\delta}\left[\frac{\partial T^*}{\partial \eta}(1, z^*)\right] \tag{49}$$

The temperature distribution in the solid-phase shell is found by solving equation (14) with boundary conditions (15) and (16). The solution to equations (14), (15), and (16) is

$$T_s = T_f + (T_f - T_w)\frac{\ln(r/\delta)}{\ln \delta^*} \tag{50}$$

and the temperature gradient in the solid at the liquid-solid interface is

$$\frac{\partial T_s}{\partial r}(\delta, z) = \frac{1}{\delta}\frac{(T_f - T_w)}{\ln \delta^*} \tag{51}$$

Substituting equations (49) and (51) into (17) and rearranging yields the following expression for the dimensionless radius of the liquid-solid interface:

$$\left[\delta^*(z^*)\right]^{1/T_w^*} = \exp\left\{-1/\left[-\frac{\partial T^*}{\partial \eta}(1, z^*)\right]\right\} \tag{52}$$

where the dimensionless parameter T_w^* is defined as

$$T_w^* = k_s(T_f - T_w)/k_L(T_o - T_f) \tag{53}$$

Therefore, the radius of the liquid-solid interface can be determined analytically through use of equations (52) and (38).

Pressure Distribution

A solution for the axial pressure distribution in the tube can be determined by means of an approximate integral form of the axial momentum equation. If equation (4) is multiplied by r and integrated from r = 0 to r = δ, and if it is assumed that p = p(z), then the following integral form results:

$$\frac{d}{dz}\int_0^{\delta} v_z^2 r\,dr + \frac{\delta}{2\rho}^2 \frac{dp}{dz} = \nu\delta \left(\frac{\partial v_z}{\partial r}(\delta, z)\right) + \nu \int_0^{\delta} \frac{\partial^2 v_z}{\partial z^2} r\,dr \qquad (54)$$

Substituting equation (19) into (54) and rearranging yields

$$\frac{1}{2\rho}\frac{dp}{dz} = \frac{4R^4V^2}{3\delta^5}\frac{d\delta}{dz} - \frac{4R^2V\nu}{\delta^4}\left[1 + \frac{1}{2}\left(\frac{d\delta}{dz}\right)^2\right] \qquad (55)$$

If the dimensionless pressure drop is defined as

$$p^* = \frac{p_o - p}{\rho V^2/2} \qquad (56)$$

then the dimensionless form of equation (55) is

$$\frac{dp^*}{dz^*} = -\frac{16}{3\delta^{*5}}\frac{d\delta^*}{dz^*} + \frac{16Pr}{\delta^{*4}}\left[1 + \frac{1}{2}\left(\frac{d\delta}{dz}\right)^2\right] \qquad (57)$$

If it is assumed that

$$\frac{1}{2}\left(\frac{d\delta}{dz}\right)^2 << 1 \qquad (58)$$

then integration of equation (57) yields

$$p^*(z^*) = \frac{4}{3\delta^{*4}}(1 - \delta^{*4}) + 16Pr\ I(z^*) \tag{59}$$

where the quantity $I(z^*)$ is defined as

$$I(z^*) = \int_0^{z^*} \frac{dz^*}{\delta^{*4}} \tag{60}$$

Therefore, the axial pressure distribution in the tube can be determined analytically through use of equations (59) and (60).

Summary of the Results

The results of the theoretical analysis presented in this chapter are summarized as follows. The rate of heat transfer from the tube is described by equations (43) and (39), the liquid bulk temperature by equation (48), the radius of the liquid-solid interface by equations (52) and (38), and the axial pressure distribution by equations (59) and (60).

Solutions to equations (38), (39), and (60) were obtained with aid of a digital computer. Equations (38) and (39), which involve infinite series, were evaluated by summing the first forty terms of the series. Equation (60), which involves an integral, was evaluated numerically by means of the Simpson method for approximating an integral. After equations (38), (39), and (60) were evaluated, solutions to equations (43), (48), (52), and (59) were obtained merely by substitution.

Solutions to the above equations are presented in a graphical form in Chapter IV, and in a tabular form in Appendix A.

CHAPTER III

EXPERIMENTAL ANALYSIS

In this chapter descriptions of the experiments devised for studying the effects of solidification of a liquid flowing through a closed conduit are presented. Two separate experiments were carried out for this purpose. The first involves the visual observation of a liquid-solid change of phase with flow through a rectangular duct. The second experiment involves the measurement of variables of interest with liquid flow through a circular tube, so that a comparison can be made between the experimental and theoretical results.

Visual Experiment

The object of the visual experiment is to observe the solidification of a liquid flowing through a closed conduit. Such observations could not only substantiate basic assumptions, but could also contribute to a better design of the second experiment involving the measurement of variables. Several questions to be answered by this experiment are:

1. What is the appearance of the solid phase shell? Does the solid phase have a monotonically increasing thickness beginning at the thermal entrance?
2. What is the physical nature of the solid phase? Is the solid phase homogeneous, smooth, and hard without the occurrance of imperfections and gaseous voids?

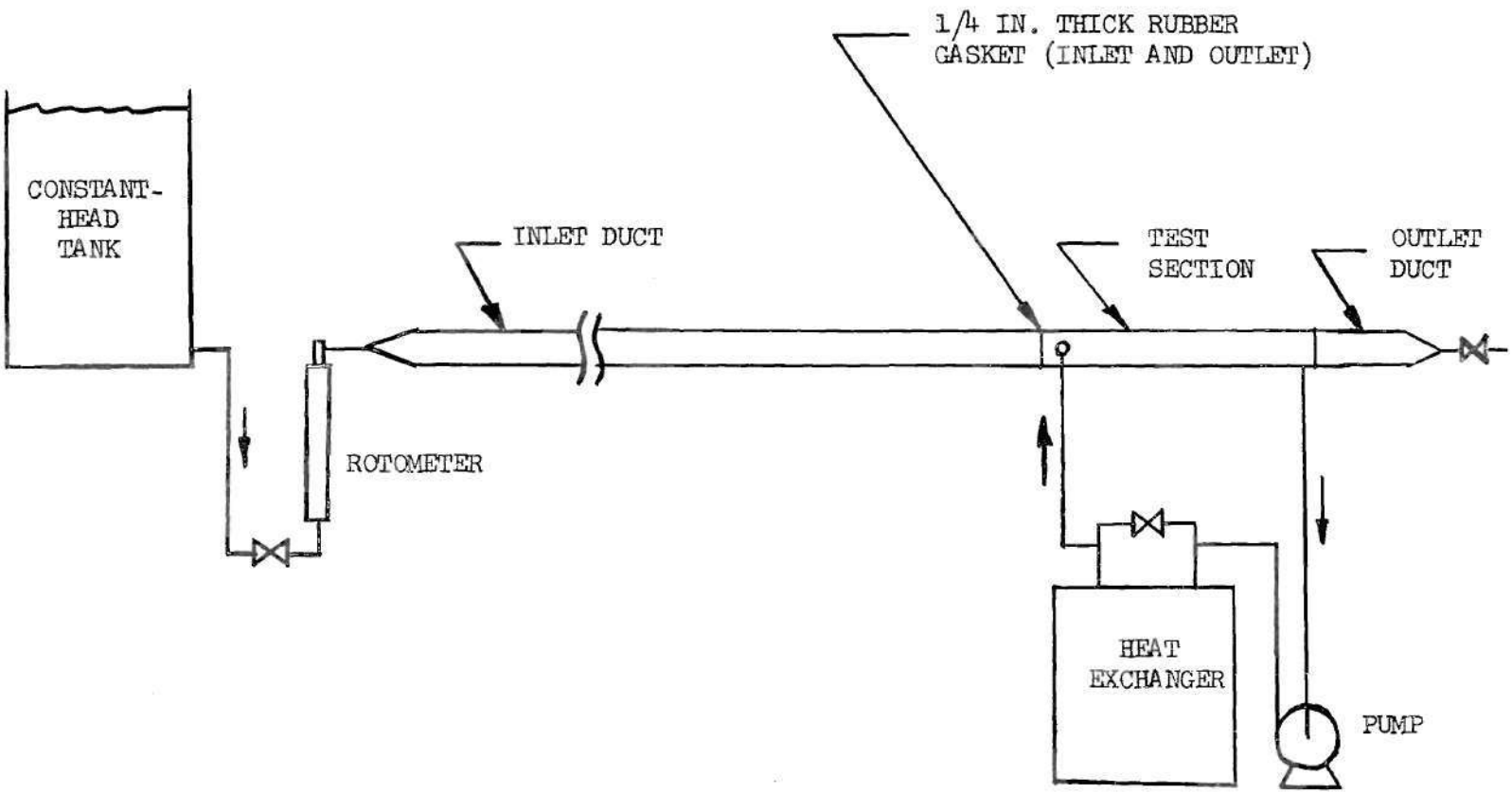

Figure 4. Visual Experiment Apparatus.

3. Approximately how much time is required for the solidification to reach steady state; i.e., when does the solid phase shell-thickness increase no more at any position along the duct?

In order to carry out the visual observation, a horizontal test section of conduit with a rectangular cross-section was constructed. The two vertical sides of the test section were made of thin copper sheets, and the two remaining sides were 1/4 inch-thick clear plexiglass strips. Water entered the test section flowing in a steady, laminar, and fully-developed manner. The entrance temperature of the water was uniform, and the copper walls of the test section were cooled and held below the freezing temperature of water.

The experimental apparatus consisted of a constant-head tank, a flowmeter, a long rectangular entrance duct, the test section, a short outlet duct with a throttling valve attached, and a heat exchanger with its associated pump and piping. A schematic diagram of the assembly is shown in Figure 4.

The function of the entrance duct was to establish a fully-developed water flow. It had a length of ten feet and a cross-section identical to the test section. The entrance duct was constructed from galvanized sheet metal. The outlet duct was similar in construction but only 18 inches long.

The test section is shown in Figure 5. Tanks constructed from galvanized sheet metal were attached to each side of the test section. Acetone was circulated through the tanks and cooling system to achieve a test section wall-temperature below the freezing temperature of water.

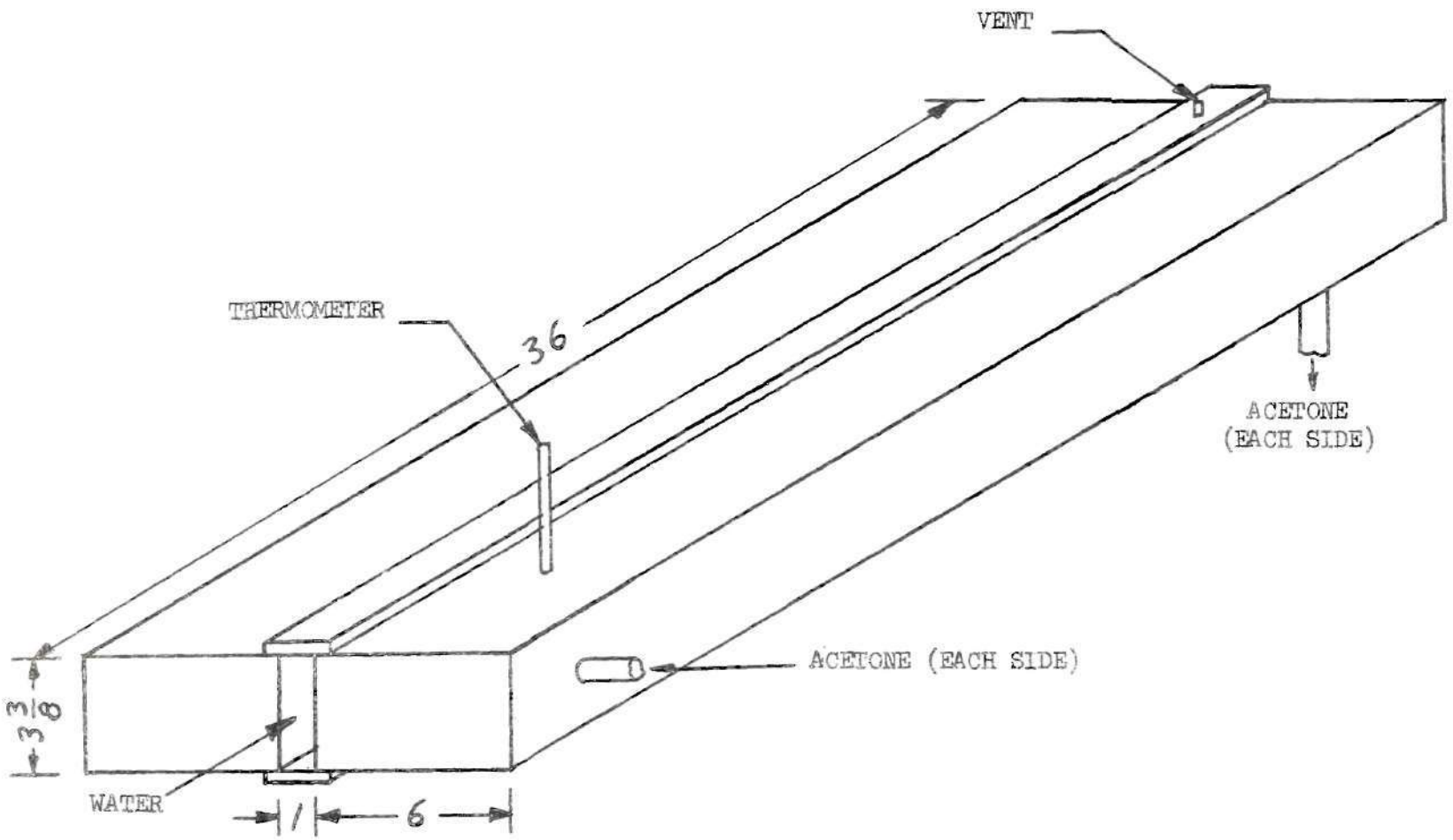

Figure 5. Visual Experiment Test Section and Coolant Tanks.

A 3/4 HP centrifugal pump circulated the acetone through the test section tanks and the heat exchanger. The heat exchanger, consisting of looped aluminum tubing, was immersed in a dry ice and acetone bath. A by-pass valve was utilized for regulating the acetone flow through the exchanger, and in this way, controlling the wall temperature of the test section.

The procedure followed in the visual experiment was to first allow the water to flow through the system at the entrance temperature. After the flow rate stabilized and all air pockets were removed, then the acetone was started to circulate through the cooling system. The temperature of the test section walls quickly dropped to a value dependent upon the regulation of the by-pass valve in the cooling system. Ice then began to form on the test-section copper walls. Eventually a steady-state condition was reached when the rate of heat transfer from the water was equal to the rate of heat transfer through the ice, and the formation of ice was thus halted.

A discussion of the observations made during the visual experiment is presented in Chapter IV.

Circular Tube Experiment

The purpose of the circular tube experiment is to measure variables which enable a comparison to be made between the experimental and theoretical results of this investigation. In order to make this comparison, it was endeavored to have the following conditions exist as nearly as possible within the experimental system:

1. The flow of liquid into the test section (cooling region) should be steady, laminar, fully-developed, and isothermal.

2. The tube wall-temperature in the test section should be constant and lower than the freezing temperature of the liquid flowing through the tube.

3. Steady-state conditions should be achieved.

The experimental system is shown schematically in Figure 6. The system consisted primarily of a constant-head tank, an inlet tube, two horizontal test sections of different length, outlet piping, a cooling system, two pressure taps, and two thermocouples.

The constant-head tank was used to obtain a steady flow of water into the system. It was a 55-gallon drum fitted with an overflow pipe approximately four feet above the test section and with an outlet at its bottom. Tap water was pumped into the constant-head tank from a 165-gallon, polyethylene-lined reservoir by means of a small centrifugal pump. A gate valve was situated between the constant-head tank outlet and the inlet tube.

The purpose of the inlet tube was to obtain a fully-developed flow of water into the test sections. The inlet tube was 13 feet long and was constructed from the same tubing as were the test sections. The length to diameter ratio for the inlet tube was approximately 102. A 1/8 inch I.D. pressure tap was located on the side of the inlet tube and two inches from the end nearer to the test sections. The inlet tube was insulated from its environment by a one-inch thick layer of fiberglass covered by wrappings of asbestos tape and aluminum foil.

Two test sections of different length were constructed from 1 1/2 inch, thin-walled, hard-drawn copper tubing (1.526 in. I.D., 1.627 in. O.D.) jacketed by 2 1/2 inch galvanized steel pipe. The test sections

were 29 and 82 inches long with length to diameter ratios of 19 and 53.75 respectively. Copper flanges were soldered to each end of the test sections. One-inch thick plexiglass insulators were situated between the test section copper flanges and the inlet tube and outlet pipe steel flanges. These connections are shown in Figures 7 and 8.

Interchangeability of the test sections and alignment of their connections were achieved in the following way. A steel flange, plexiglass insulator, and two copper flanges were first bolted together. Two dowel pins were then put into this assembly, and each piece was marked to indicate its position. The assembly was then placed in a lathe and a hole with the same diameter as the inside diameter of the copper tubing was bored. Then the plexiglass was removed and a hole with the same diameter as the outside diameter of the copper tubing was bored through the steel and copper flanges. This procedure was carried out for both the inlet and outlet connections.

Water leakage between the flange and plexiglass interfaces was prevented by placing small, continuous beads of Permagum sealant between them. Grooves 1/4 inch wide, 1/8 inch deep, and with an inside diameter of 2 1/4 inch, cut into the plexiglass faces, accumulated any excess sealant and thus prevented the sealant from squeezing into the water passageway.

The test sections, end connections, and outlet piping were insulated in the same manner as the inlet tube.

The outlet piping consisted of a 1 1/2 in. steel nipple, a 1 1/2 in. steel elbow reduced to a 3/8 in. steel nipple, a 3/8 in. throttling valve, and finally another 3/8 in. steel nipple. A pressure probe constructed from 1/8 in. O.D. and 1/4 in. O.D. copper tubing was inserted into the liquid passageway through a hole drilled in the elbow. The

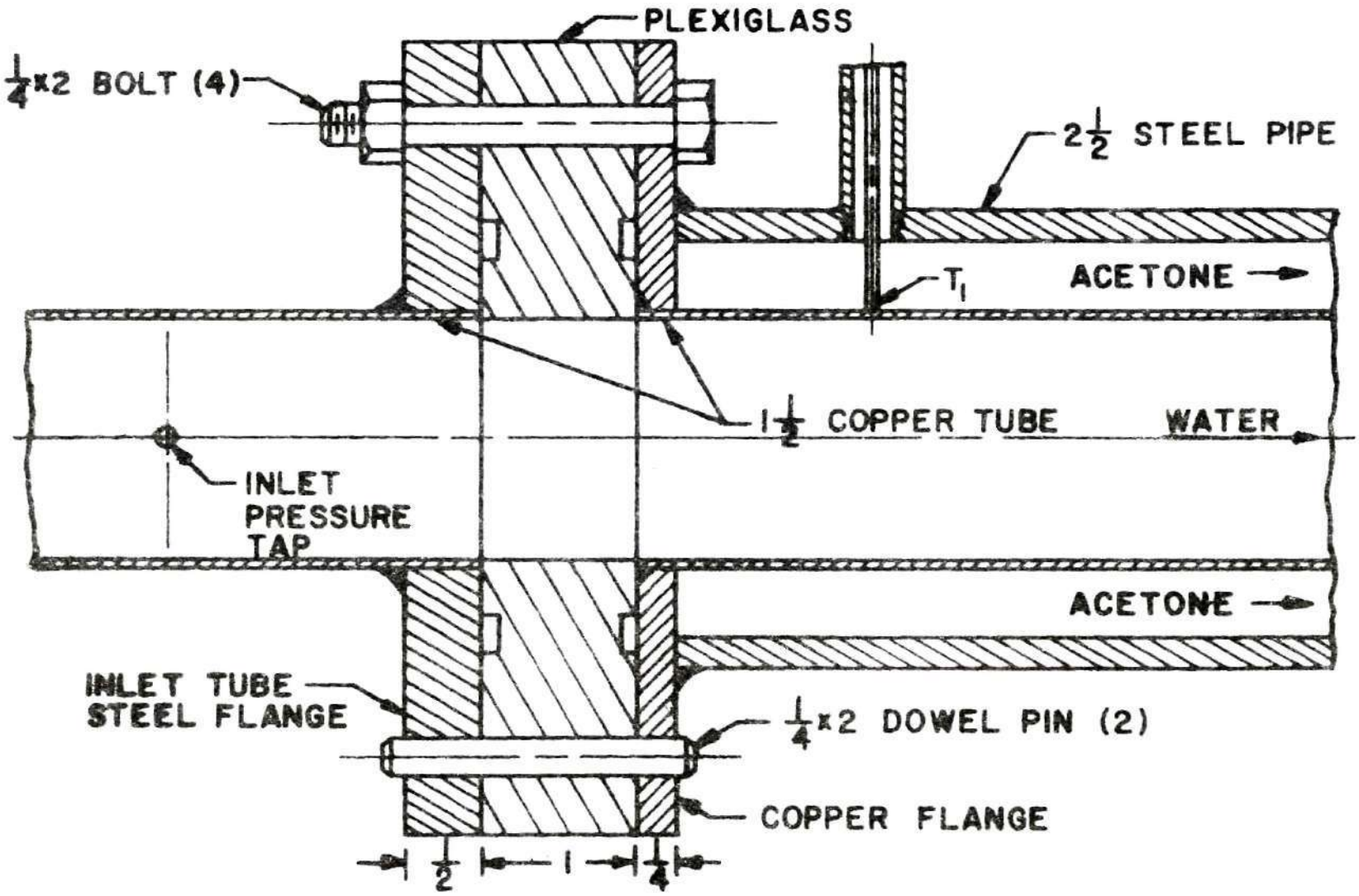

Figure 7. Test Section Inlet Connection.

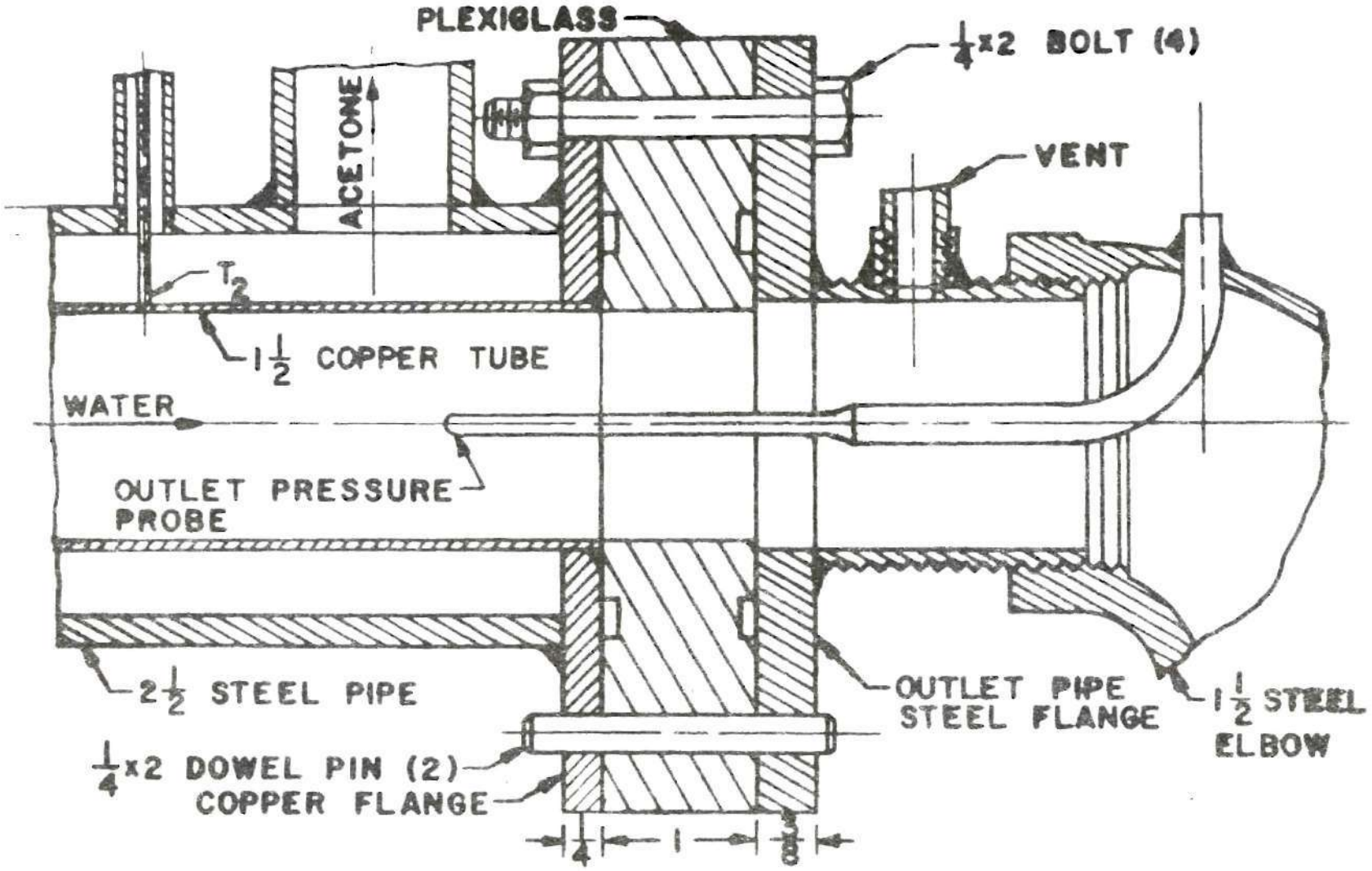

Figure 8. Test Section Outlet Connection.

probe is also shown in Figure 8. It had a solid blunt tip, and four 0.040 in. holes were drilled around its circumference one inch from the tip. When the probe was inserted into the water passageway, these holes were located at the test section outlet.

The test section tube wall-temperature was measured by two Minneapolis-Honeywell, six-inch, Mego-Pak, Type T thermocouples. Thermocouple T_1 entered the test section through the top and rested against the tube wall 1 1/2 inch from the test section inlet. Thermocouple T_2 was positioned in the same manner as T_1, but was located 3 inches from the test section outlet. The thermocouple voltages were determined by means of a Leeds and Northrup millivolt potentiometer (Cat. No. 8686, G.I.T. 81594). The thermocouple readings were compared with a standard thermometer (Scientific Glass Apparatus Co., No. 1024, Range -10 to +60°C in 0.2°) at the ice point and at room temperature, and agreed within 0.1°C. It is believed that these thermocouples have an error less than 0.2°C throughout the temperature range experienced in this investigation.

Acetone from the cooling system entered the annular space of the test section horizontally at each side and 1 1/2 inch from the test section inlet. After flowing through the annular space at a high flow rate, the acetone exited through the top of the annular space 1 1/2 inches from the test section outlet.

The cooling system consisted of a one HP centrifugal pump, heat exchanger, by-pass gate valve, and 1/2 in. motorized throttling valve. The pump circulated acetone through the heat exchanger and by-pass line into the test section annular space. The by-pass and motorized valves, acting together, regulated the acetone flow through the exchanger, and

in this way, controlled the tube wall-temperature in the test section. The heat exchanger was simply looped aluminum tubing immersed in a dry ice and acetone bath. The heat exchanger consummed approximately 30 pounds of dry ice per hour.

The motorized valve was driven by a Minneapolis-Honeywell M930B Actionator motor. Thermocouple T_1 was connected to a Honeywell-Brown Electronic strip chart proportional controller with an integrally mounted Electr-O-Line control unit (G.I.T. 82138). The control unit operated the motorized valve, keeping the temperature T_1 within $\pm 0.1^{\circ}C$ of a value preset on the controller.

The pressure drop of the water flowing through the test section was determined by measuring the difference in the vertical height of water columns connected to the inlet pressure tap and the outlet pressure probe. A Gaertner Scientific Corporation cathetometer (G.I.T. 28191), which can be read to the nearest 0.005 cm., was used to make this measurement. It is estimated that the pressure drop across the test section was determined with an error less than 0.010 inch of water.

The water temperature in the constant-head tank, T_o, the bulk temperature of the water leaving the system, T_b, and the mass flowrate of the water were measured in addition to T_1, T_2, and the pressure drop across the test section.

Temperatures T_o and T_b were measured with the standard thermometer. T_o was determined by simply immersing the thermometer into the tank, and T_b was determined by immersing the thermometer into a Dewar flask into which the water from the system was flowing. In order to check the methods of measuring T_o, T_b, T_1, and T_2, water approximately $5^{\circ}C$ lower

than the ambient temperature was allowed to pass through the apparatus while the cooling system was not in operation. This test confirmed the reliability of the temperature measurements, since all readings agreed.

The mass flowrate of the water was determined by measuring with a stopwatch the time required to fill a one-gallon bottle. The filled bottle was then weighed on a balance which can be read to the nearest 0.01 pound. It is estimated that mass flowrate measurements made in this manner had an error of less than one per cent.

The procedure employed for obtaining data in the circular tube experiment was as follows. Before each series of runs, water to be used was allowed to stand in the constant-head tank and reservoir for at least 12 hours. This permitted air to leave the water and allowed the water temperature to become very nearly equal to the ambient temperature. Then the motorized valve controller was adjusted to a desired test section tube wall-temperature, and water was started flowing through the system. After the water flow stabilized at a desired flow rate, the cooling system pump was started and time allowed for each of the temperature readings (T_o, T_b, T_1, and T_2) to become constant. Then the temperatures, mass flowrate, and pressure drop across the test section (when sufficiently large to be measured accurately) were recorded. The water flowrate was then decreased, and time was again allowed for steady-state conditions to be reached before new readings were recorded. This procedure was repeated for a series of flowrates and test section tube wall-temperatures.

Experimental runs were made with tube wall-temperatures both lower and slightly higher than the freezing temperature of water. This

permitted a very important evaluation of the effect of natural convection and variable fluid properties, and enabled their interaction with solidification effects to be properly assessed.

A discussion of the results of the circular tube experiment is presented in Chapter IV, properties of water and ice are presented in Appendix B, and experimental data are presented in a tabular form in Appendix C.

CHAPTER IV

RESULTS

Theoretical Analysis

Numerical results of the analysis presented in Chapter II are shown graphically in Figures 9 and 10. The dimensionless bulk temperature T_b^*, the dimensionless radius of the liquid-solid interface δ^* with the reciprocal of the parameter T_w^* as an exponent, and the dimensionless heat transfer rate q^* are plotted versus the dimensionless axial position variable z^* in Figure 9. These curves show that as z^* increases, the liquid bulk temperature and radius of the liquid-solid interface decrease, and the heat transfer rate increases. Also, if the parameter T_w^* is increased, then the radius of the liquid-solid interface is decreased. The numerical results for T_b^* are computed from equation (48), results for $(\delta^*)^{1/T_w^*}$ are computed from equations (52) and (38), and results for q^* are computed from equations (43) and (39).

In Figure 10 the dimensionless pressure drop p^* is plotted versus z^* for values of the Prandtl Number equal to 5.0 and 10.0, and for T_w^* equal to 0.5, 1.0, and 2.0. These curves illustrate how p^* is increased when z^*, Pr, or T_w^* is increased. The numerical results for p^* are computed from equations (59) and (60).

The most notable result of the theoretical analysis is that the dimensionless bulk temperature and heat transfer rate (with solidification) are independent of the tube wall-temperature and radius of the liquid-solid interface. Therefore, if T_b^* and q^* for the case of T_w

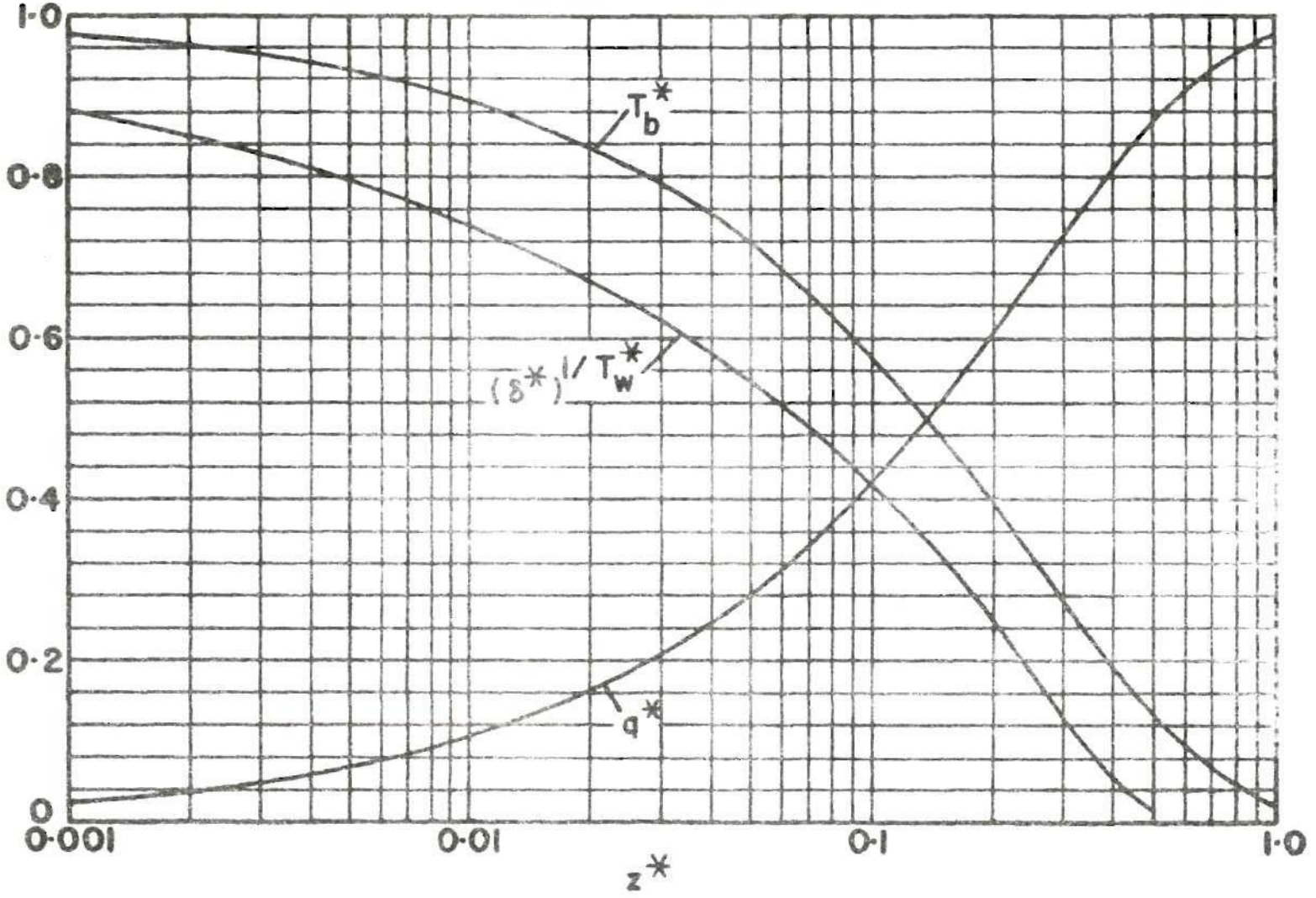

Figure 9. Theoretical Dimensionless Bulk Temperature, Heat Transfer, and Radius of the Liquid-Solid Interface.

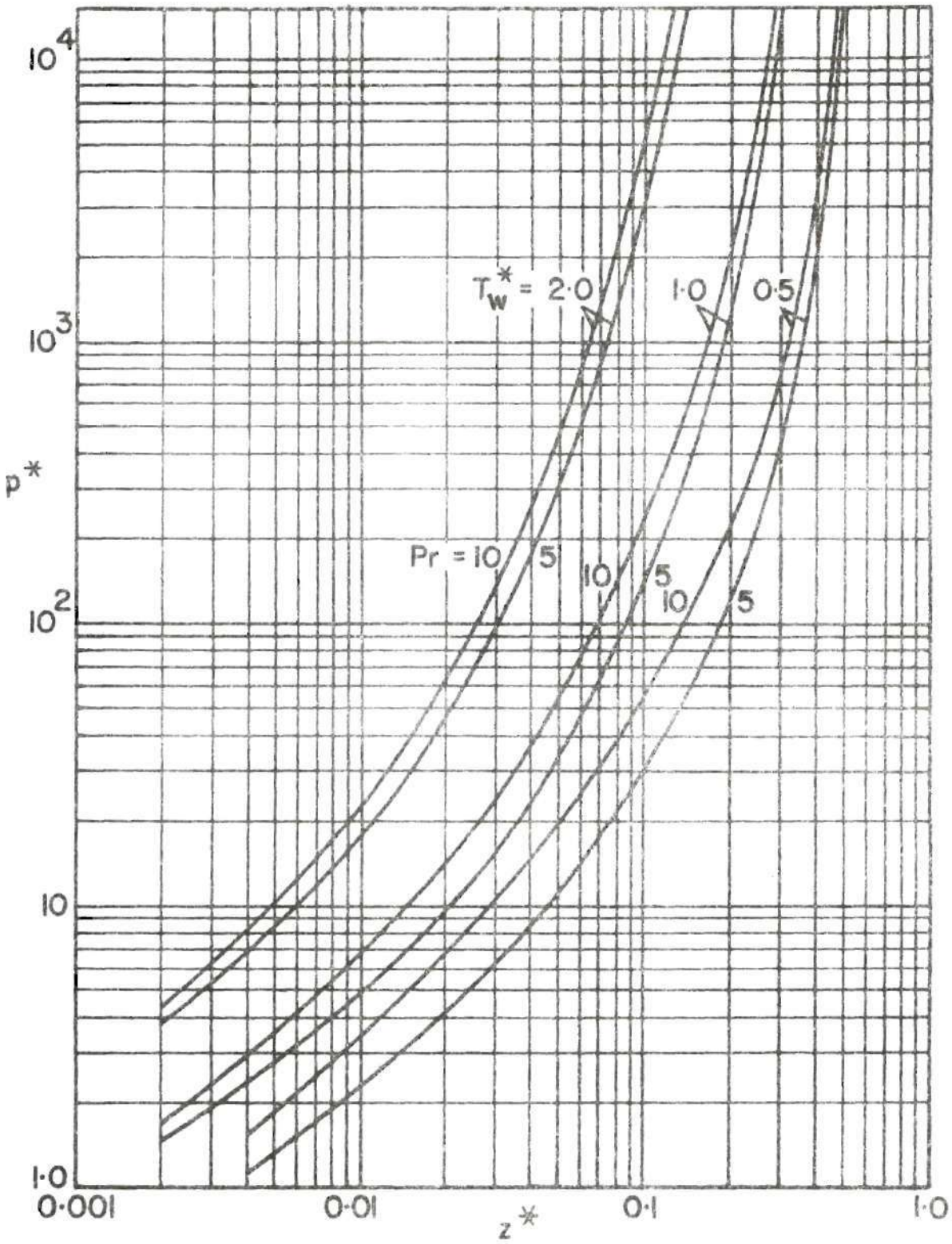

Figure 10. Theoretical Pressure Drop versus Axial Position.

greater than T_f (no solidification) are defined as

$$T_b^* = (T_b - T_w)/(T_o - T_w) \tag{61}$$

$$q^* = q/\pi R^2 V \rho c_p (T_o - T_w) \tag{62}$$

then the dimensionless bulk temperature and heat transfer curves of Figure 9 also represent solutions to the Graetz problem.

Visual Experiment

The object of the visual experiment is to observe the solidification of water flowing through the test section described in Chapter III. A photograph of an ice-shell profile formed within the test section under steady-state conditions is shown in Figure 11, and a labeled sketch of the photograph is shown in Figure 12. The photograph is taken from above the test section, while looking toward the test section inlet. Floodlights placed above and below the test section illuminate the water passageway.

Conditions within the experimental apparatus at the time of the photograph were as follows: Water temperature at the test section inlet was about 55°F; acetone temperature in the test section tanks was about 10°F; water flowrate from the constant-head tank was about 0.5 gallon per minute; and the Reynolds Number in the inlet duct, based on the hydraulic diameter, was about 470.

The photograph shows a gradual increase of the ice thickness beginning at the test section inlet, and a very smooth appearance of the ice-water interfaces. The ice was observed to be hard, clear, and homogeneous except for the presence of a small amount of air bubbles

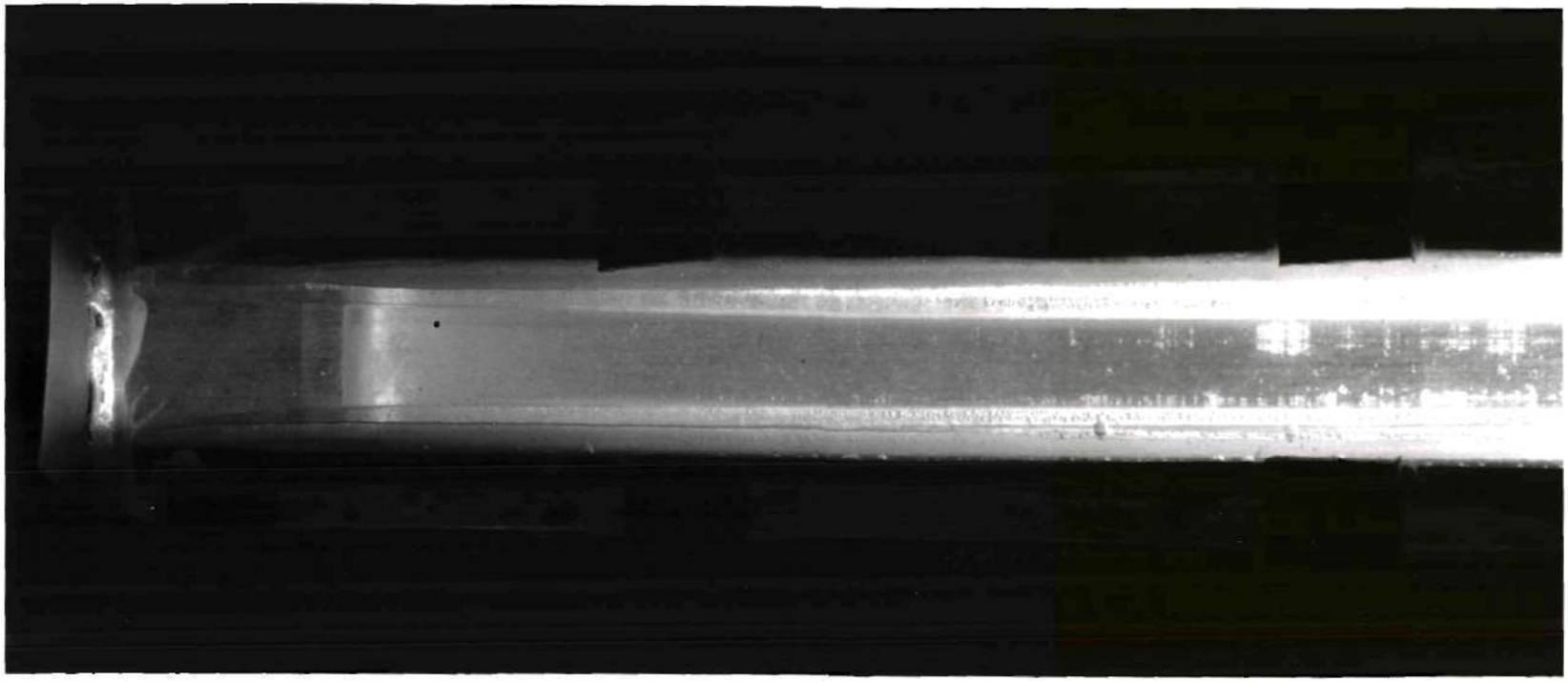

Figure 11. Photograph of Ice-Shell Profile within Test Section of Visual Experiment.

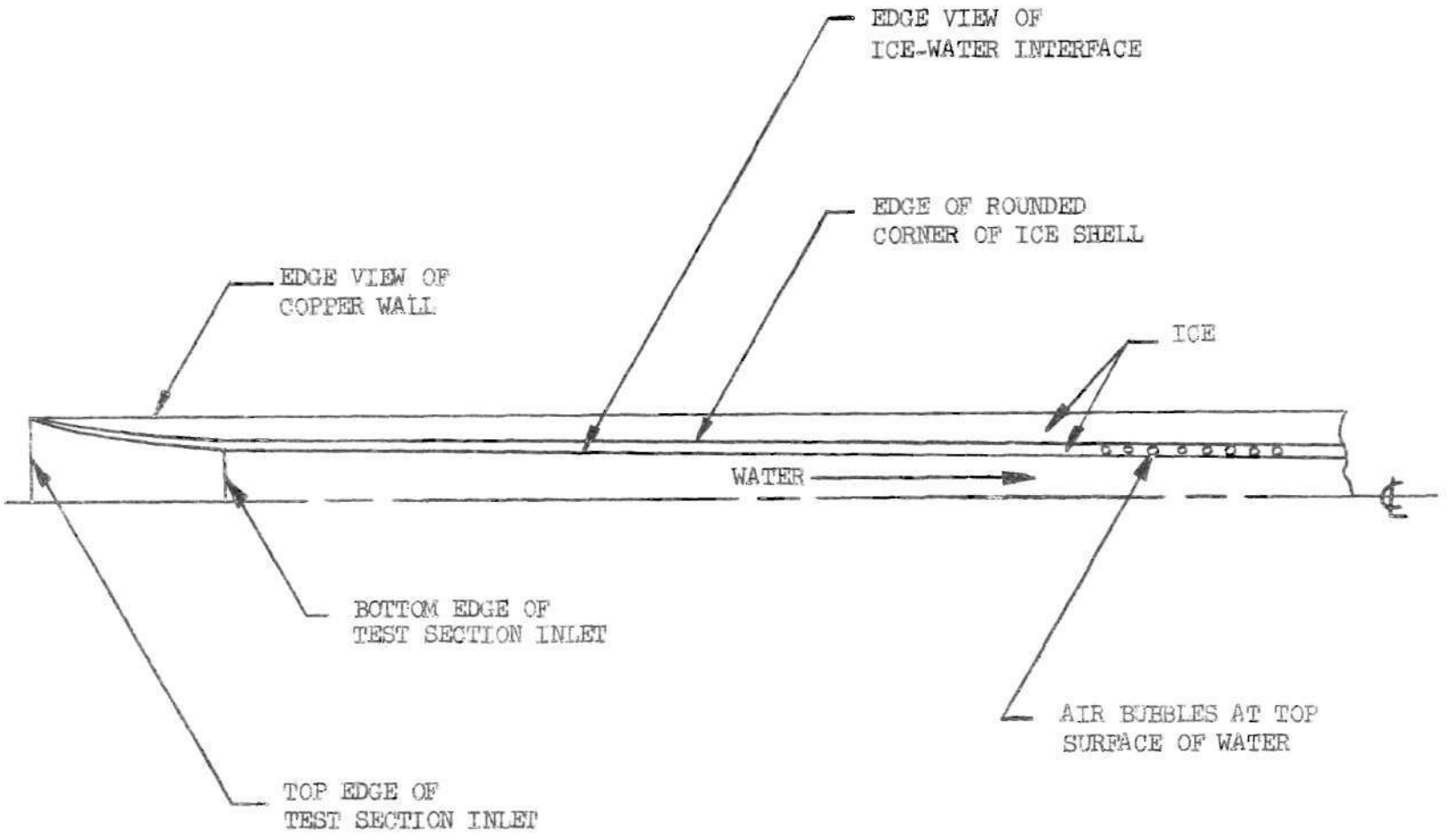

Figure 12. Sketch of Ice-Shell Profile within Test Section of Visual Experiment.

within the ice. The volume of the air bubbles relative to the ice volume was negligible. The hardness of the ice was verified by an attempt to scratch its surface with a piece of wire, which was inserted through the air vent.

A labeled sketch of the photograph is given in Figure 12. The sketch shows an edge view of one copper wall and, since the photograph is taken from an angle, the top and bottom edges of the test section inlet. Since the temperature of the plexiglass top and bottom walls was not held below the water freezing temperature, the ice-water interface had rounded top and bottom corners. The edge of the rounded top corner is shown in the sketch along with an edge view of the ice-water interface. Air bubbles which floated to the top surface of the water are also shown.

The ice formation along the entire length of the test section required approximately 20 to 30 minutes to reach the steady-state condition. This time interval was estimated by simply observing when the growth of the ice-shell thickness had apparently stopped.

In general, the observations made during the visual experiment substantiated basic assumptions concerning the character and appearance of the solid-phase shell. The visual experiment was also helpful by contributing to the design of the apparatus and to the formulation of the procedure used in the circular tube experiment.

Circular Tube Experiment

The purpose of the circular tube experiment described in Chapter III is to measure variables which enable a comparison to be made between the experimental and theoretical results of this investigation. The

variables used for this comparison are dimensionless bulk temperature and dimensionless pressure drop. Plots of the experimental data and theoretical results are shown in Figure 13 and 14. The experimental data are given in a tabular form in Appendix C.

The experimental and theoretical dimensionless bulk temperatures T_b^* are plotted versus the dimensionless axial position variable z^* in Figure 13. Curves A, B, and C represent data taken from the test section with an L/D of 19; and curves D, E, and F represent data taken from the test section with an L/D of 53.75.

Curves A and D represent data taken with tube wall-temperatures slightly warmer than the freezing temperature of water (no solidification). Therefore, the difference existing between the theoretical curve and the curves A and D is due to the effect of natural convection and variable properties, which increases heat transfer and, thereby, lowers bulk temperature.

Curves B, C, E, and F represent data taken with tube wall-temperatures colder than the freezing temperature of water. Therefore, the difference existing between these curves and curves A or D is due solely to the effect of solidification.

The tube wall-temperatures of curves C and F are colder than those of curves B and E. Since curves C and F lie above B and E, this illustrates that increased solidification reduces the effect of natural convection, and results in a corresponding reduction of heat transfer and increase of bulk temperature. It is apparent that this increase of bulk temperature with increase of solidification is greater for larger z^* (larger z/D or lower mass flowrates), and in the case of curve F,

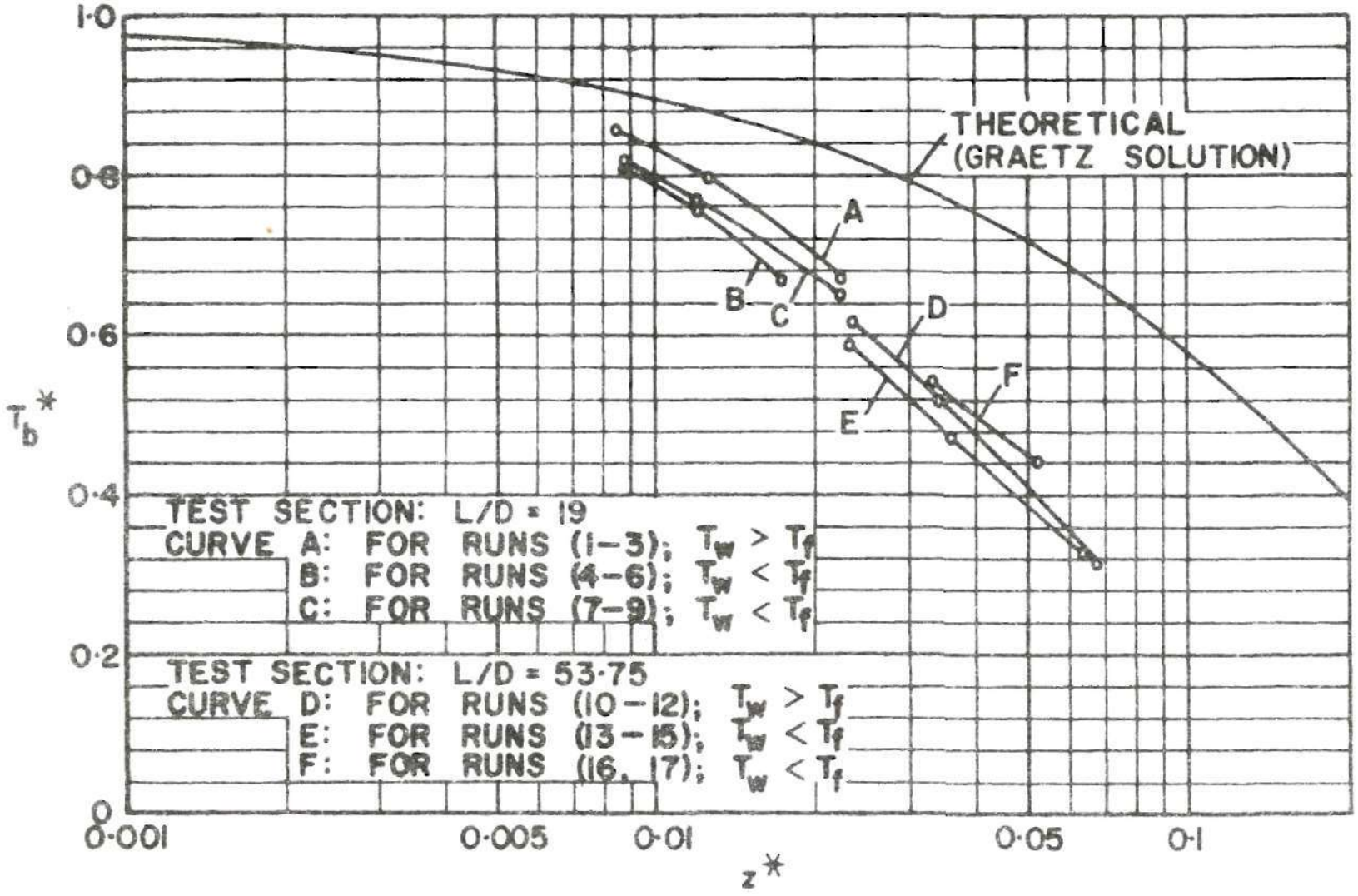

Figure 13. Comparison of Experimental and Theoretical Dimensionless Bulk Temperature.

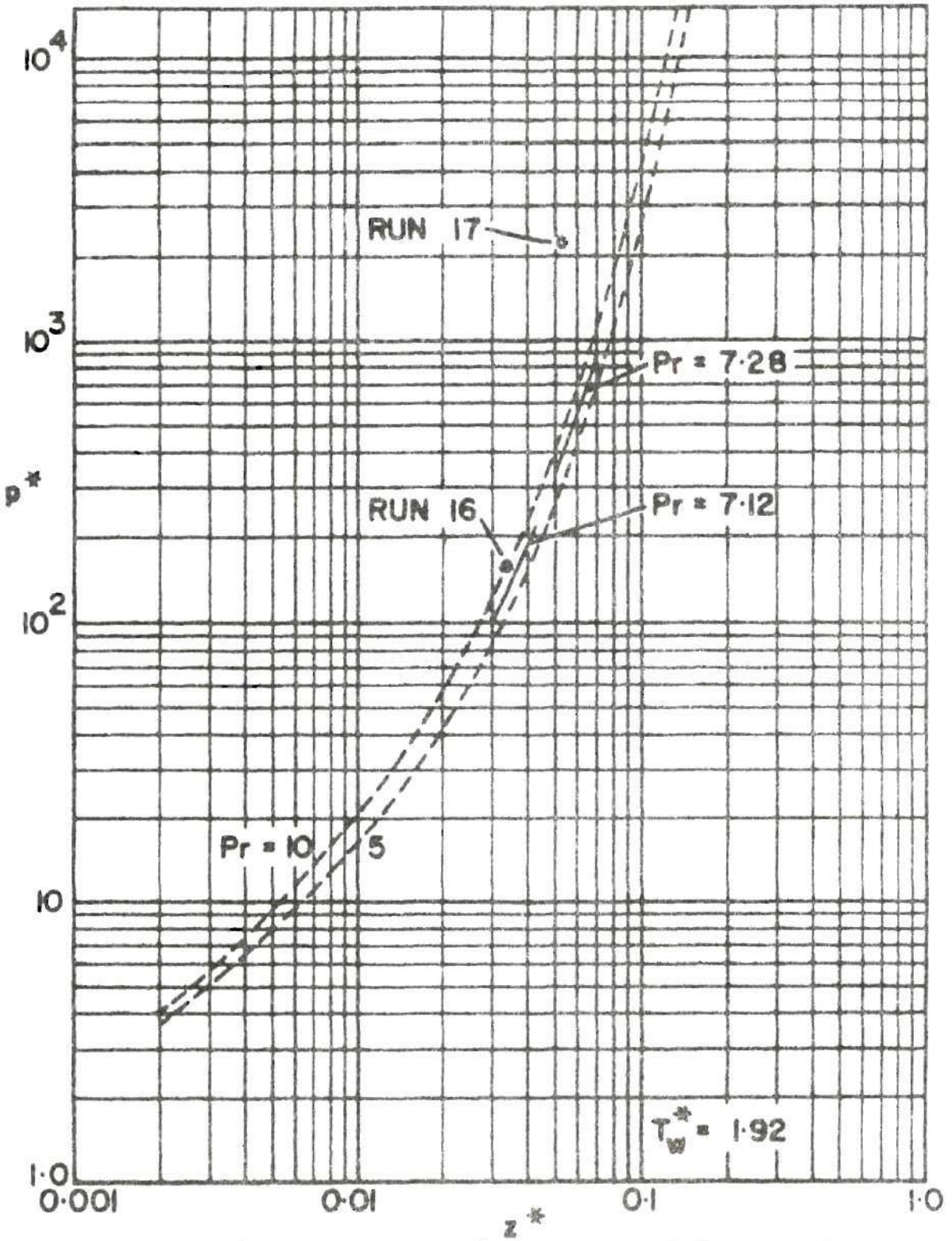

Figure 14. Comparison of Experimental and Theoretical Dimensionless Pressure Drop.

the bulk temperature is increased to such an extent that it lies above curve D.

An equation relating the radius of the liquid-solid interface to bulk temperature is derived in Appendix D. It is

$$(\delta^*)^{1/T_w^*} = \exp\left[2/\frac{dT_b^*}{dz^*}\right] \tag{63}$$

Equation (63) shows that the radius of the liquid-solid interface is a function of the gradient of the bulk temperature distribution. The gradient is negative with a value of minus infinity at the tube thermal entrance. It increases as z increases, and approaches a value of zero corresponding to complete closure of the tube by the solid phase.

The effect of natural convection upon the radius of the liquid-solid interface can be discussed through the implications of equation (63). Near the entrance to the cooling region, natural convection combined with solidification cools the liquid bulk temperature lower than what is theoretically predicted. Therefore, the bulk temperature gradient is smaller, which means that the radius of the liquid-solid interface is larger than what is theoretically predicted. But further along the tube, solidification and fluid acceleration tend to offset natural convection, and a position is reached where the bulk temperature gradient is larger than what is theoretically predicted. Beyond this position, the radius of the liquid-solid interface is smaller than the theoretical result. Thus, the overall effect of natural convection upon the solid-phase shell is to make it thinner at small z^* and thicker at large z^*, than what is theoretically predicted.

A comparison of theoretical dimensionless pressure drop p^* and experimental results for runs 16 and 17 is shown in Figure 14. Theoretical results are plotted for a T_w^* of 1.92 and for Prandtl Numbers of 5.0, 7.12, 7.28, and 10.0. Experimental measurements for run 16 are $p^* = 160$, $z^* = 0.0333$, $Pr = 7.12$, and $T_w^* = 1.92$; and for run 17 they are $p^* = 2240$, $z^* = 0.0526$, $Pr = 7.28$, and $T_w^* = 1.92$.

The theoretical p^* values corresponding to runs 16 and 17 are 130 and 400, with respective errors of -19 and -82 per cent. The fact that the experimental values of p^* are greater than the theoretical predictions can be partially attributed to the effect of natural convection currents upon the water flow. Combined forced and natural convection in horizontal tubes produces a spiraling flow which increases viscous shear and pressure drop. Another factor is that since the effect of natural convection on solidification at large z^* is to constrict the flow area even more than what is theoretically predicted, the pressure drop should be correspondingly larger than the theoretical results. This reasoning would explain the large pressure measurements of experimental runs 16 and 17, expecially since the per cent error is greater for run 17 at the larger z^*.

In general, the comparison between the theoretical results and data taken from the circular tube experiment shows that natural convection can produce a wide variance in results. It also demonstrates that the theoretical result for T_b^* is an upper bound for liquid solidification in circular tubes, the theoretical result for δ^* is an upper bound at large z^*, and the theoretical result for p^* is a lower bound at large z^*. Equation (63) further implies that if the bulk temperature distribution in a circular tube with liquid solidification

can be predicted or closely approximated, then the solid-phase shell profile can be determined. Such an approximation, considering the effect of natural convection within the folowing liquid, is presented in the following section.

Semi-Empirical Solution

If the bulk temperature distribution in a circular tube with liquid solidification can be predicted or closely approximated, then the solid-phase shell profile can be determined through use of equation (63).

One method of solution is to approximate the bulk temperature distribution with empirical results for fluid flow without solidification. Thus, natural convection within the flowing liquid is taken into consideration.

An empirical equation due to Oliver (14) for laminar, fully-developed flow entering a circular tube is suitable for such a solution. It is

$$(Nu)_{am} = 1.75F_1(\mu_a/\mu_w)^{0.14}\left[\pi/z^* + 5.6\times10^{-4}(Gr\ Pr\ z/D)^{0.7}\right]^{1/3} \qquad (64)$$

where

$$F_1 = z^*(Nu)_{am}\ln(T_b^*) \qquad (65)$$

$$T_b^* = \frac{2 - z^*(Nu)_{am}}{2 + z^*(Nu)_{am}} \qquad (66)$$

The material properties occurring in equation (64) are to be evaluated at the average of the inlet and bulk temperatures, except for μ_w, which is to be evaluated at the tube wall-temperature. The temperature difference

in the Grashof Number is defined as the average of the inlet and bulk temperatures minus the tube wall-temperature. Derivations of the relationships between T_b^*, q^*, and $(Nu)_{am}$ are given in Appendix E.

A comparison between circular tube data with no solidification and results calculated from equations (64-66) is shown in Figure 15. The difference between the calculated and experimental dimensionless bulk temperatures ranges from 1.4 to 7.3 per cent.

In order to illustrate how natural convection affects the solid-phase shell profile, a semi-empirical solution was carried out for the following hypothetical problem: Water enters the cooling region of a tube (1.526 in I.D.) with a temperature of 28°C, and the tube wall-temperature is colder than the freezing temperature of water so that an ice shell is formed at the tube inner surface.

Equations (64-66) were used to calculate the bulk temperature distributions shown in Figure 16 for inlet Reynolds Numbers of 500, 1000, and 1500. Since the bulk temperature curves are intended to approximate those for the above hypothetical problem, a tube wall-temperature equal to the freezing temperature of water was assumed for the calculations. The difference between the Graetz solution and the curves A, B, and C of Figure 16 is due to the effect of natural convection and variable properties.

Numerical results for the radius of the ice-water interface, corresponding to the bulk temperature curves A, B, C of Figure 16, are plotted as curves D, E, F in Figure 17. The numerical results were obtained by approximating the bulk temperature curves of Figure 16 with a series of second degree polynomials, and then substituting the gradients of the polynomials into equation (63). The gradients of the bulk

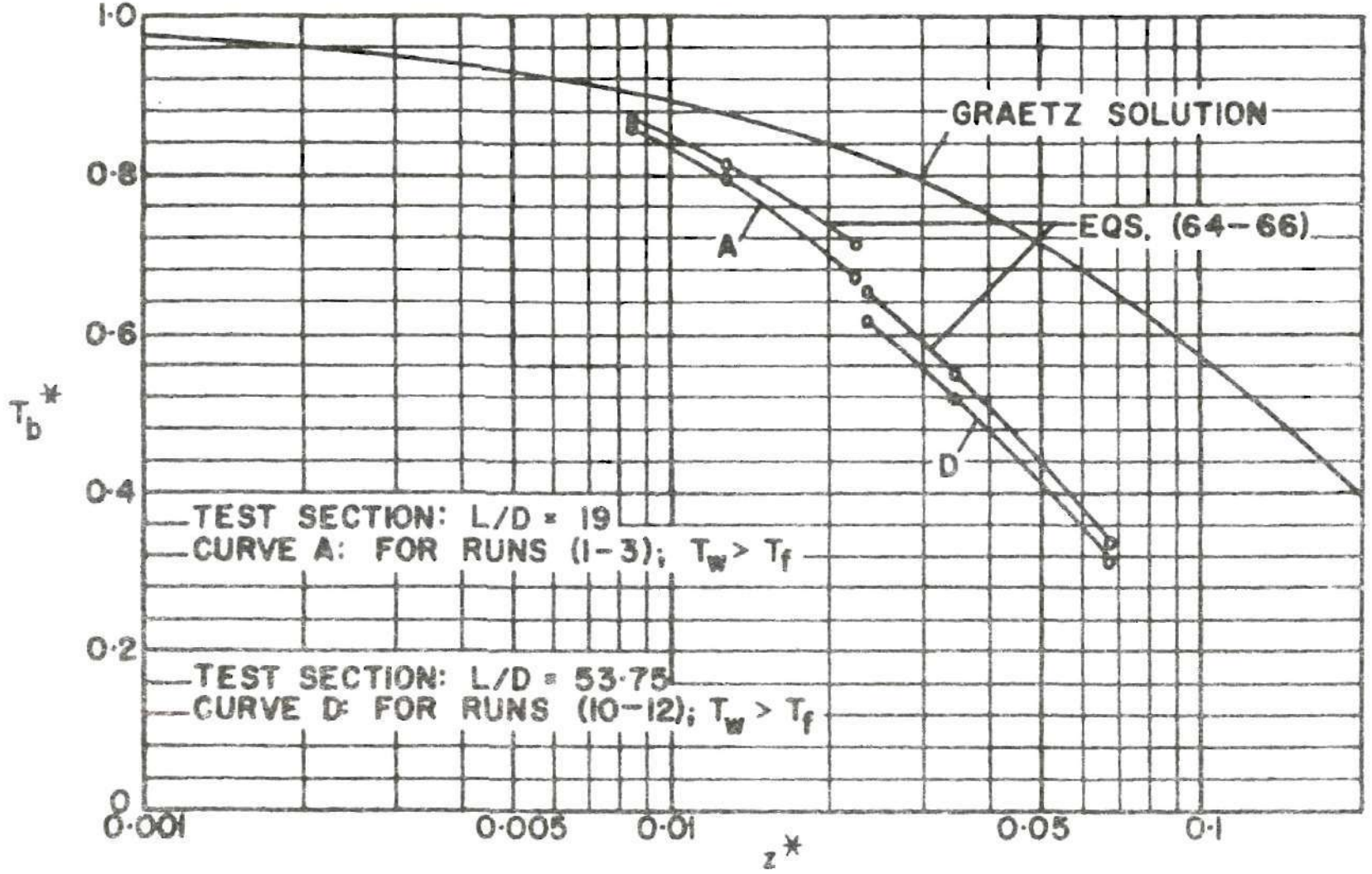

Figure 15. Comparison of Experimental Data and Calculated Results Using Equations (64-66).

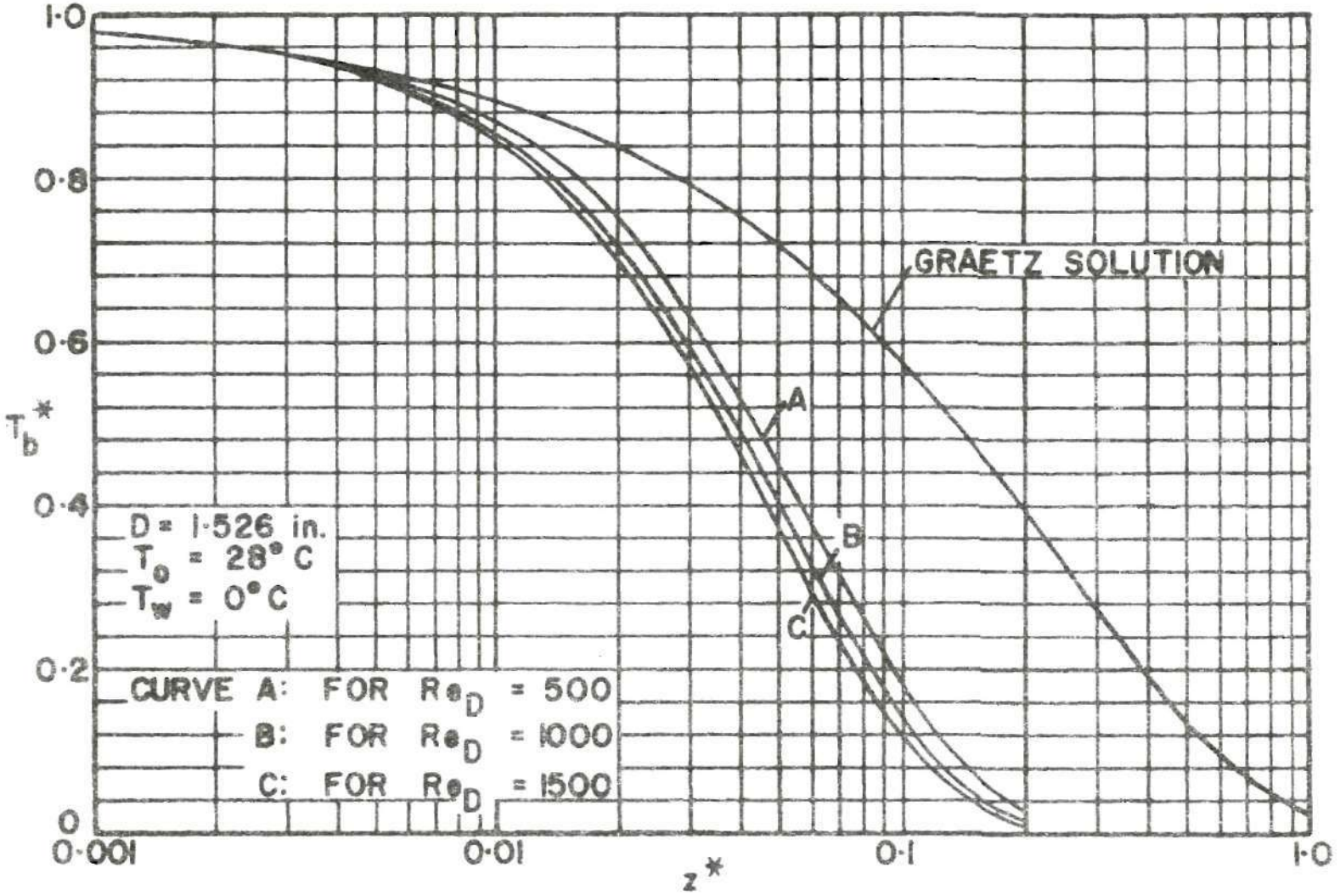

Figure 16. Bulk Temperature Distribution for Water Flow in a Tube with No Solidification.

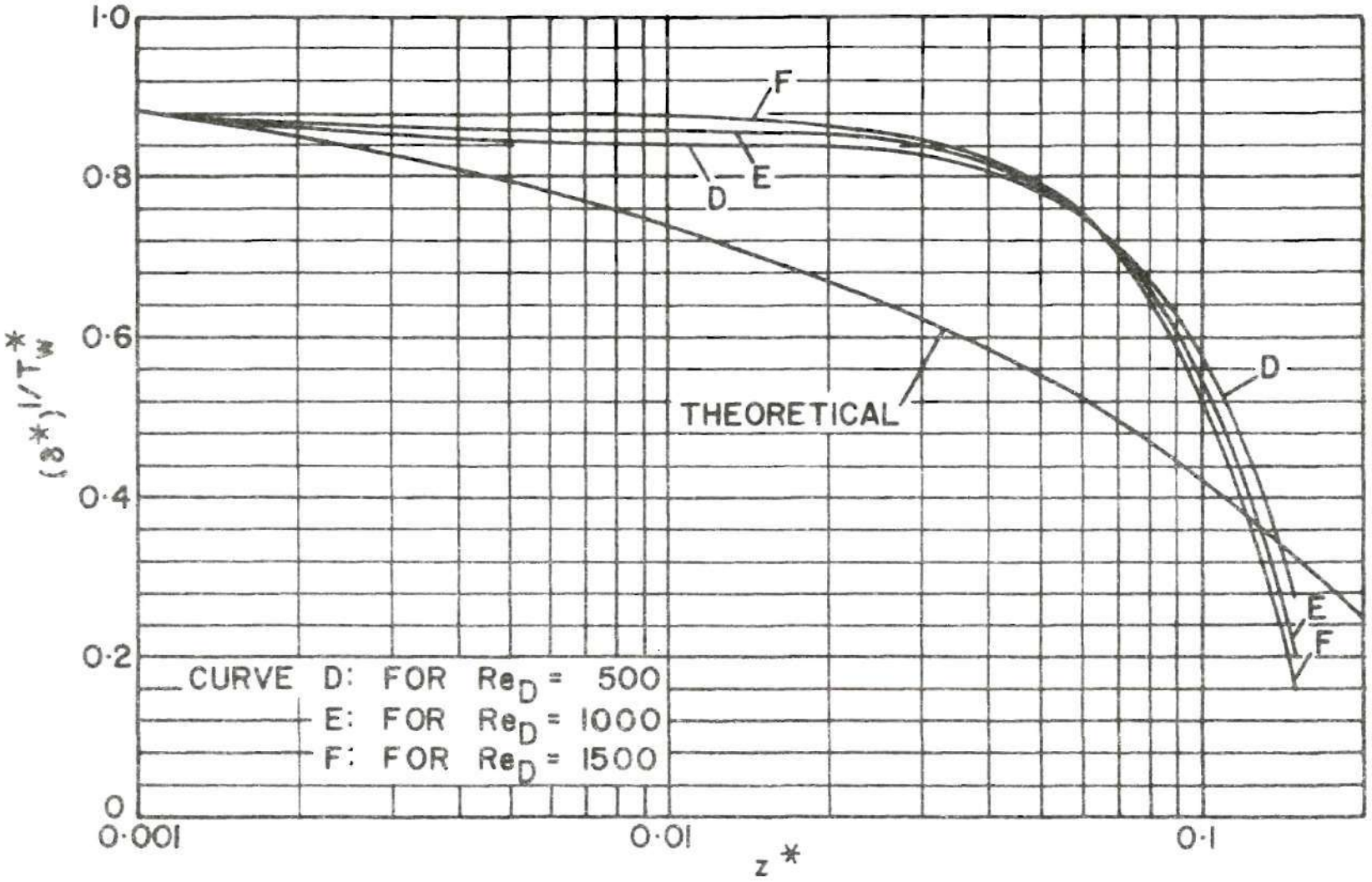

Figure 17. Comparison of Theoretical and Semi-Empirical Results for the Radius of the Liquid-Solid Interface.

temperature curves could also have been determined graphically or by approximating the bulk temperature curves with a series of first or higher order polynomials.

The semi-empirical curves D, E, and F of Figure 17 illustrate very well the effect of natural convection upon the radius of the liquid-solid interface. The curves lie above the theoretical curve for small z^*, and fall below the theoretical curve for large z^*. Since solidification reduces natural convection effects at large z^*, curves corresponding to the actual solution of the hypothetical problem would lie below curves D, E, and F. Thus, the semi-empirical solution gives a valuable upper bound to the radius of the liquid-solid interface at large z^*.

The semi-empirical method presented in this section not only illustrates how natural convection affects the solid-phase shell profile, but also provides, for large z^*, an upper bound which is even closer to the actual solution than the theoretical results.

CHAPTER V

CONCLUSIONS

The effect of liquid solidification at the inner surface of a circular tube upon laminar-flow heat transfer and pressure drop has been investigated analytically and experimentally for steady-state conditions.

Theoretical expressions for the bulk temperature distribution, heat transfer rate, radius of the liquid-solid interface, and pressure drop have been determined from a mathematical analysis. In the mathematical analysis it is assumed that natural convection within the flowing liquid is negligible. The experimental results show that if natural convection is not negligible, then a considerable variance between the theoretical and experimental results can exist.

Since the theoretical solution for combined forced and natural convection is extremely difficult to obtain, a semi-empirical method for obtaining approximate solutions is developed, which accounts for the added effect of natural convection. This method can be used for either laminar or turbulent flow and for fluids other than Newtonian liquids.

CHAPTER VI

RECOMMENDATIONS

The literature survey prior to this investigation revealed that very little research has been accomplished with regard to the solidification of a material flowing in a duct. This means that a host of problems can be recommended for future study. Among these are analytical and experimental studies involving isothermal, convection, or radiation boundary conditions with laminar, turbulent, or pulsating flow of a liquid, gas, solution, or non-Newtonian fluid in a horizontal or vertical duct under transient or steady-state conditions.

It is hoped that the results and observations reported in this investigation will provide a suitable foundation for future related investigations.

APPENDIX A

TABULATED THEORETICAL RESULTS

The eigenvalues λ_n and constants $(-C_n R_n'(1)/2)$, which were used to evaluate equations (38) and (39), appear in Table 1. They are reproduced from Sellers, et al. (5).

Table 1. Eigenvalues and Constants Occurring in the Graetz Problem

n	λ_n	$(-C_n R_n'(1)/2)$
0	2.7043644	0.74879
1	6.679032	0.54424
2	10.67338	0.46288
3	14.67108	0.41518
4	18.66987	0.38237

For n greater than 4,

$$\lambda_n = 4n - 8/3$$

$$(-C_n R_n'(1)/2) = 1.01276(\lambda_n)^{-1/3}$$

The dimensionless heat transfer from the tube q^*, and the dimensionless liquid bulk temperature T_b^* are tabulated in Table 2 for various values of the dimensionless tube length z^*. The values for q^* and T_b^* were computed from

$$\int_0^{z^*} \left[- \frac{\partial T^*}{\partial \eta} (1, z^*) \right] dz^* = 4 \sum_{n=0}^{\infty} \left[-C_n R_n'(1)/2 \right] (\lambda_n)^{-2} \left[1 - \exp(-\lambda_n^2 z^*/2) \right] \tag{39}$$

$$q^* = 2\int_0^{z^*} \left[-\frac{\partial T^*}{\partial \eta}(1,z^*)\right] dz^* \tag{43}$$

$$T_b^* = 1 - q^* \tag{48}$$

Table 2. Dimensionless Heat Transfer and Liquid Bulk Temperature Versus Dimensionless Tube Length

z^*	q^*	T_b^*
0.001	0.02267	0.97733
0.0025	0.04240	0.95760
0.005	0.06703	0.93297
0.01	0.10480	0.89520
0.025	0.18591	0.81409
0.05	0.28214	0.71786
0.1	0.41949	0.58051
0.2	0.60299	0.39701
0.3	0.72473	0.27527
0.5	0.86670	0.13330
0.7	0.93496	0.06504
1.0	0.97715	0.02285

The dimensionless temperature gradient in the liquid at the liquid-solid interface, and the dimensionless radius of the liquid-solid interface are tabulated in Table 3 for various values of the dimensionless tube length z^*. The values for the dimensionless temperature gradient and radius of the liquid-solid interface were computed from

$$\left[-\frac{\partial T^*}{\partial \eta}(1,z^*)\right] = 2\sum_{n=0}^{\infty} \left[-C_n R_n'(1)/2\right] \exp(-\lambda_n^2 z^*/2) \tag{38}$$

$$\left[\delta^*(z^*)\right]^{1/T_w^*} = \exp\left\{-1\Big/\left[-\frac{\partial T^*}{\partial \eta}(1,z^*)\right]\right\} \tag{52}$$

Table 3. Dimensionless Temperature Gradient in the Liquid and Radius of the Liquid-Solid Interface Versus Dimensionless Axial Position

z^*	$-\frac{\partial T^*}{\partial \eta}(1,z^*)$	$\left[\delta^*(z^*)\right]^{1/T_w^*}$
0.001	7.92869	0.88151
0.002	6.16403	0.85024
0.003	5.30499	0.82820
0.004	4.76170	0.81058
0.005	4.37440	0.79564
0.006	4.07840	0.78255
0.007	3.84159	0.77081
0.008	3.64590	0.76012
0.009	3.48024	0.75026
0.010	3.33735	0.74109
0.02	2.50976	0.67136
0.03	2.10441	0.62177
0.04	1.84660	0.58185
0.05	1.66179	0.54785
0.06	1.51973	0.51788
0.07	1.40541	0.49089
0.08	1.31036	0.46620
0.09	1.22937	0.44334
0.10	1.15902	0.42198
0.11	1.09697	0.40188
0.12	1.04152	0.38284
0.13	0.99144	0.36472
0.14	0.94579	0.34739
0.15	0.90384	0.33075
0.16	0.86503	0.31473
0.17	0.82889	0.29926
0.18	0.79508	0.28430
0.19	0.76329	0.26979
0.20	0.73330	0.25571
0.21	0.70490	0.24204
0.22	0.67794	0.22877
0.23	0.65228	0.21587
0.24	0.62780	0.20334
0.25	0.60441	0.19119
0.26	0.58203	0.17940

Table 3. (Continued)

z^*	$-\frac{\partial T^*}{\partial \eta}(1,z^*)$	$\left[\delta^*(z^*)\right]^{1/T_w^*}$
0.27	0.56059	0.16799
0.28	0.54003	0.15696
0.29	0.52029	0.14631
0.30	0.30133	0.13606
0.31	0.48311	0.12619
0.32	0.46558	0.11674
0.33	0.44872	0.10769
0.34	0.43250	0.09905
0.35	0.41688	0.09083
0.36	0.40184	0.08303
0.37	0.38735	0.07565
0.38	0.37339	0.06869
0.39	0.35995	0.06215
0.40	0.34699	0.05603
0.41	0.33451	0.05032
0.42	0.32248	0.04501
0.43	0.31089	0.04009
0.44	0.29971	0.03556
0.45	0.28894	0.03140
0.46	0.27856	0.02760
0.47	0.26855	0.02414
0.48	0.25890	0.02102
0.49	0.24960	0.01820
0.50	0.24063	0.01567

The integral $I(z^*)$ is tabulated in Tables 4, 5, 6, and 7 for T_w^* equal to 0.5, 1.0, 1.92, and 2.0. The values for $I(z^*)$ were obtained by application of the Simpson method of approximating an integral to the relation

$$I(z^*) = \int_0^{z^*} \frac{dz^*}{\left[\delta(z^*)\right]^4} \tag{60}$$

Table 4. $I(z^*)$ for $T_w^* = 0.5$

z^*	$I(z^*)$	z^*	$I(z^*)$
0.002	0.002510	0.23	1.82541
0.004	0.005422	0.25	2.31061
0.006	0.008580	0.27	2.93419
0.008	0.011945	0.29	3.74923
0.01	0.015498	0.31	4.83451
0.03	0.044272	0.33	6.30963
0.05	0.10338	0.35	8.36013
0.07	0.17804	0.37	11.28067
0.09	0.27018	0.39	15.55196
0.11	0.38265	0.41	21.97851
0.13	0.51932	0.43	31.95329
0.15	0.68533	0.45	47.95232
0.17	0.88763	0.47	74.55656
0.19	1.13561	0.49	120.51667
0.21	1.44222		

Table 5. $I(z^*)$ for $T_w^* = 1.0$

z^*	$I(z^*)$	z^*	$I(z^*)$
0.002	0.003179	0.23	21.16608
0.004	0.007423	0.25	32.99494
0.006	0.012411	0.27	52.54721
0.008	0.018075	0.29	85.97445
0.01	0.024387	0.31	145.3002
0.03	0.098981	0.33	255.0195
0.05	0.27461	0.35	467.3000
0.07	0.55438	0.37	898.5915
0.09	0.98033	0.39	1822.6967
0.11	1.61491	0.41	3918.8784
0.13	2.55176	0.43	8980.7394
1.15	3.93420	0.45	22038.677
0.17	5.98724	0.47	58260.983
0.19	9.07297	0.49	166755.23
0.21	13.79192		

Table 6. $I(z^*)$ for $T_w^* = 1.92$

z^*	$I(z^*)$	z^*	$I(z^*)$
0.002	0.005004	0.13	60.2322
0.004	0.013506	0.15	129.0958
0.006	0.025085	0.17	276.3233
0.008	0.039859	0.19	598.5343
0.01	0.058042	0.21	1327.8074
0.03	0.44582	0.23	3048.8804
0.05	1.76617	0.25	7321.4847
0.07	4.97990	0.27	18561.735
0.09	12.16942	0.29	50124.55
0.11	27.61282	0.31	145400.54

Table 7. $I(z^*)$ for $T_w^* = 2.0$

z^*	$I(z^*)$	z^*	$I(z^*)$
0.002	0.005210	0.13	80.0906
0.004	0.014243	0.15	176.8752
0.006	0.026703	0.17	390.4637
0.008	0.042762	0.19	873.4525
0.01	0.062698	0.21	2004.5950
0.03	0.50889	0.23	4771.7037
0.05	2.08370	0.25	11907.641
0.07	6.05997	0.27	31456.967
0.09	15.25734	0.29	88779.62
0.11	35.65168	0.31	270021.25

The dimensionless axial pressure drop $p^*(z^*)$ for values of the Prandtl Number equal to 1.0, 5.0, and 10.0 is tabulated in Tables 8, 9, and 10 for T_w^* equal to 0.5, 1.0, and 2.0. The values $p^*(z^*)$ were computed from

$$p^*(z^*) = 4(1 - \delta^{*4})/3\delta^{*4} + 16\mathrm{Pr}\, I(z^*) \qquad (59)$$

Table 8. Dimensionless Pressure Drop Versus Dimensionless Axial Position for $T_w^* = 0.5$

	$p^*(z^*)$		
z^*	Pr = 1.0	Pr = 5.0	Pr = 10
0.002	0.55125	0.71189	0.91269
0.004	0.78265	1.1295	1.5631
0.006	0.98008	1.5292	2.2156
0.008	1.1654	1.9296	2.8848
0.01	1.3424	2.3344	3.5744
0.03	2.8233	5.6566	9.1982
0.05	4.7588	11.375	19.646
0.07	7.0388	18.433	32.676
0.09	9.7727	27.064	48.673
0.11	13.045	37.534	68.146
0.13	16.999	50.235	91.781
0.15	21.819	65.680	120.50
0.21	44.501	136.81	252.18
0.31	159.74	469.15	855.91
0.41	877.01	2283.7	4042.0
0.49	5953.2	13667	23308

Table 9. Dimensionless Pressure Drop Versus Dimensionless Axial Position for $T_w^* = 1.0$

	$p^*(z^*)$		
z^*	Pr = 1.0	Pr = 5.0	Pr = 10
0.002	1.2690	1.4724	1.7267
0.004	1.8739	2.3489	2.9428
0.006	2.4208	3.2151	4.2080
0.008	2.9500	4.1068	5.5528
0.01	3.4772	5.0380	6.9889
0.03	9.1714	15.506	23.425
0.05	17.862	35.437	57.406
0.07	30.499	65.998	110.33
0.09	48.864	111.60	190.03
0.11	75.618	178.97	308.16
0.13	114.85	278.16	482.30
0.15	173.03	424.82	739.55
0.21	607.83	1490.5	2593.9
0.31	7581.4	16881	28505

Table 10. Dimensionless Pressure Drop Versus Dimensionless Axial Position for $T_w^* = 2.0$

z^*	$p^*(z^*)$		
	Pr = 1.0	Pr = 5.0	Pr = 10
0.002	3.6322	3.9656	4.3824
0.004	6.0483	6.9597	8.0989
0.006	8.5750	10.284	12.420
0.008	11.315	14.052	17.473
0.01	14.325	18.338	23.354
0.03	66.493	99.062	139.77
0.05	196.31	329.67	496.36
0.07	491.08	878.92	1363.7
0.09	1136.1	2112.6	3333.1
0.11	2528.6	4810.4	7662.5
0.13	5538.8	10665	17072
0.15	12139	23449	37609

APPENDIX B

PROPERTIES OF WATER AND ICE

Property values for water and ice, which were used in the experimental analysis, are tabulated in Tables 11 and 12 for various temperatures. The property values are taken from Dorsey (25), and are valid at a pressure of 1 atm. The density values are taken from Table 93 (section III) of reference (25), the viscosity from Table 82, the specific heat at constant pressure from Table 113, the coefficient of volumetric expansion from Table 97, the thermal conductivity of water from Table 130 (data of Barratt and Nettleton), and the thermal conductivity of ice from Table 208 (data of Jacob and Erk).

Table 11. Properties of Water

T	ρ	μ	c_p	$\beta \times 10^4$	k_L
^oC	$\frac{lbm}{ft^3}$	$\frac{lbm}{hr\text{-}ft}$	$\frac{B}{lbm\text{-}^oF}$	$\frac{1}{^oC}$	$\frac{B}{hr\text{-}ft\text{-}^oF}$
0	62.42	4.340	1.008		0.320
5	62.43	3.675	1.004		0.325
10	62.41	3.169	1.001	0.939	0.330
15	62.38	2.770	1.000		0.3345
20	62.32	2.441	0.999	2.00	0.339
25	62.24	2.163	0.998		0.344
30	62.16	1.935	0.998	2.94	0.349

Table 11. (Continued)

T ^{o}C	$\nu \times 10^5$ $\frac{ft^2}{sec}$	$\alpha \times 10^5$ $\frac{ft^2}{sec}$	Pr
0	1.931	0.1414	13.66
5	1.635	0.1440	11.35
10	1.411	0.1465	9.63
15	1.234	0.1490	8.28
20	1.088	0.1514	7.19
25	0.965	0.1538	6.28
30	0.865	0.1561	5.54

Table 12. Thermal Conductivity of Ice

T, ^{o}C	0	-10	-20	-30
k_s, B/hr-ft-^{o}F	1.294	1.341	1.404	1.474

APPENDIX C

CIRCUIAR TUBE EXPERIMENTAL DATA

Experimental data for water flow in tubes with length to diameter ratios of 19 and 53.75 are tabulated in Tables 13 and 14. In the tables T_w appears as the average of T_1 and T_2, Re_D is the inlet Reynolds Number, and the material properties occurring in z^* and Pr are evaluated at the average of T_o and T_b. The thermal conductivity of ice occurring in T_w^* is evaluated at the average of T_w and $T_f(0^oC)$, and the thermal conductivity of water occurring in T_w^* is evaluated at the average of $(T_o + T_b)/2$ and T_f.

Table 13. Experimental Data for Water Flow in a Horizontal Tube with L/D = 19

Run	T_1 ^oC	T_2 ^oC	T_w ^oC	T_b ^oC	T_o ^oC
1	0.40	2.20	1.3	24.8	28.7
2	0.40	2.20	1.3	23.3	28.9
3	0.79	2.33	1.6	20.0	29.0
4	-7.21	-5.90	-6.6	22.5	27.8
5	-7.08	-5.90	-6.5	21.0	27.7
6	-7.08	-5.50	-6.3	18.6	27.7
7	-19.70	-15.62	-17.7	23.2	28.4
8	-19.70	-15.89	-17.8	21.5	28.0
9	-19.43	-16.70	-18.1	18.3	28.2

Table 13. (Continued)

Run	$\dot{m}$ lbm/min	Re_D	z^*	T_b^*	T_w^*
1	5.19	1561	0.00846	0.857	--
2	3.43	1040	0.01275	0.797	--
3	1.92	583	0.0226	0.672	--
4	4.96	1470	0.00879	0.810	0.934
5	3.61	1064	0.01207	0.758	0.923
6	2.46	725	0.01762	0.671	0.896
7	4.95	1493	0.00883	0.817	2.50
8	3.62	1078	0.01201	0.768	2.56
9	1.92	574	0.0226	0.649	2.59

Table 14. Experimental Data for Water Flow in a Horizontal Tube with L/D = 53.75

Run	T_1 °C	T_2 °C	T_w °C	T_b °C	T_o °C
10	0.58	2.59	1.6	17.9	28.0
11	0.58	2.59	1.6	15.4	28.2
12	0.66	1.69	1.2	9.6	28.0
13	-8.00	-5.37	-6.7	15.4	26.2
14	-8.00	-5.37	-6.7	12.5	26.4
15	-7.71	-6.16	-6.9	8.8	26.9
16	-13.74	-11.61	-12.7	14.3	26.5
17	-13.87	-12.13	-13.0	12.0	27.2

Table 14. (Continued)

Run	(p_o-p) in.H_2O	Pr	p^*
16	0.177	7.12	160
17	0.990	7.28	2240

Table 14. (Continued)

Run	$\dot{m}$ lbm/min	Re_D	z^*	T_b^*	T_w^*
10	5.18	1540	0.0237	0.618	--
11	3.54	1060	0.0345	0.519	--
12	1.783	530	0.0679	0.314	--
13	5.18	1477	0.0235	0.588	1.01
14	3.37	966	0.0360	0.474	1.01
15	1.892	546	0.0639	0.327	1.02
16	3.65	1047	0.0333	0.541	1.92
17	2.31	672	0.0526	0.441	1.92

APPENDIX D

DERIVATION OF THE EQUATION RELATING δ^* TO T_b^*

An equation relating the radius of the liquid-solid interface in a tube with solidification to the gradient of the bulk temperature is presented in Chapter IV. It is

$$(\delta^*)^{1/T_w^*} = \exp\left[2/\frac{dT_b^*}{dz^*}\right] \tag{63}$$

Equation (63) is derived as follows. From an energy balance applied to a tube of length z

$$\pi R^2 V \rho c_p T_o = \int_0^z \left[-k_s \frac{\partial T_s}{\partial r}(R,z)\right] 2\pi R dz + \rho c_p \int_0^\delta T v_z 2\pi r dr \tag{67}$$

Bulk temperature is defined as

$$T_b = \frac{2}{R^2 V} \int_0^\delta T v_z r dr \tag{45}$$

Combining equations (67) and (45) and solving for T_b yields

$$T_b = T_o + \frac{2k_s}{RV\rho c_p} \int_0^z \left[\frac{\partial T_s}{\partial r}(R,z)\right] dz \tag{68}$$

An equation for the temperature distribution in the solid phase is

$$T_s = T_f + (T_f - T_w)\frac{\ln(r/\delta)}{\ln \delta^*} \tag{50}$$

and the temperature gradient in the solid phase at the tube wall is

$$\frac{\partial T_s}{\partial r}(R,z) = \frac{T_f - T_w}{R \ln \delta^*} \tag{69}$$

Substituting equation (69) into (68) and nondimensionalizing yields

$$T_b^* = 1 + 2T_w^* \int_0^{z^*} \frac{dz^*}{\ln \delta^*} \tag{70}$$

Differentiation of equation (70) gives

$$\frac{dT_b^*}{dz^*} = \frac{2T_w^*}{\ln \delta^*} \tag{71}$$

and rearranging equation (71) yields the desired relation

$$(\delta^*)^{1/T_w^*} = \exp\left[2 / \frac{dT_b^*}{dz^*}\right] \tag{63}$$

Equation (63) can be used for either laminar or turbulent flow, and for fluids other than Newtonian liquids. The primary assumptions are negligible axial heat conduction, constant density and specific heat, and a temperature distribution in the solid phase which can be suitably described by equation (50).

APPENDIX E

DERIVATION OF THE RELATIONSHIPS BETWEEN T_b^*, q^*, AND $(Nu)_{am}$

Without Solidification

The relation between T_b^* and q^* without solidification is derived as follows. From an energy balance applied to a tube of length z

$$\pi R^2 V \rho c_p T_o = q + \rho c_p \int_0^R T v_z 2\pi r dr \tag{72}$$

The liquid bulk temperature is defined as

$$T_b = \frac{2}{R^2 V} \int_0^R T v_z r dr \tag{45}$$

Combining equations (72) and (45) and solving for T_b yields

$$T_b = T_o - q/\pi R^2 V \rho c_p \tag{73}$$

The dimensionless bulk temperature T_b^* and heat transfer rate q^* without solidification are defined as

$$T_b^* = (T_b - T_w)/(T_o - T_w) \tag{61}$$

$$q^* = q/\pi R^2 V \rho c_p (T_o - T_w) \tag{62}$$

Rearranging equation (73) into the form of equation (61) and substituting equation (62) gives the following relation between T_b^* and q^*:

$$T_b^* = 1 - q^* \tag{74}$$

The relation between q^* and $(Nu)_{am}$ without solidification is derived as follows. The arithmetic mean heat transfer coefficient for a circular tube of length z is defined as

$$h_{am} = q/\pi Dz \left[(T_b + T_o)/2 - T_w\right] \tag{75}$$

Combining equations (62) and (75) yields

$$q^* = \frac{h_{am} D z}{2R^2 V \rho c_p} \left[(T_b - T_w)/(T_o - T_w) + 1\right] \tag{76}$$

The arithmetic mean Nusselt Number is defined as

$$(Nu)_{am} = h_{am} D/k \tag{77}$$

Combining equations (24), (61), (77), and (76) yields

$$q^* = z^*(Nu)_{am}(T_b^* + 1)/2 \tag{78}$$

Substituting equation (74) into (78) and solving for q^* gives the following relation between T_b^* and $(Nu)_{am}$:

$$q^* = 2z^*(Nu)_{am}/\left[2 + z^*(Nu)_{am}\right] \tag{79}$$

Substituting equation (74) into (79) and solving for T_b^* gives the following relation between T_b^* and $(Nu)_{am}$ without solidification:

$$T_b^* = \left[2 - z^*(Nu)_{am}\right] / \left[2 + z^*(Nu)_{am}\right] \tag{80}$$

With Solidification

The relation between T_b^* and q^* with solidification is derived in Chapter II. It is

$$T_b^* = 1 - q^* \tag{48}$$

where

$$T_b^* = (T_b - T_f)/(T_o - T_f) \tag{47}$$

$$q^* = q/\pi R^2 V \rho c_p (T_o - T_f) \tag{42}$$

The relation between q^* and $(Nu)_{am}$ with solidification is derived as follows. If the arithmetic mean heat transfer coefficient for a tube of length z with solidification is defined as

$$h_{am} = q/\pi Dz \left[(T_b + T_o)/2 - T_f\right] \tag{81}$$

then combining equations (42) and (81) yields

$$q^* = \frac{h_{am} Dz}{2R^2 V \rho c_p} \left[(T_b - T_f)/(T_o - T_f) + 1\right] \tag{82}$$

If the arithmetic mean Nusselt Number is defined by equation (77) with or without solidification, then combining equations (24), (47), (77), and (82) yields

$$q^* = z^*(Nu)_{am}(T_b^* + 1)/2 \tag{83}$$

Substituting equation (48) into (83) and solving for q^* gives the following relation between q^* and $(Nu)_{am}$:

$$q^* = 2z^*(Nu)_{am} / \left[2 + z^*(Nu)_{am}\right] \qquad (84)$$

Substituting equation (48) into (84) and solving for T_b^* gives the following relation between T_b^* and $(Nu)_{am}$ with solidification:

$$T_b^* = \left[2 - z^*(Nu)_{am}\right] / \left[2 + z^*(Nu)_{am}\right] \qquad (85)$$

It can be seen that if q^*, T_b^*, h_{am}, and $(Nu)_{am}$ are defined by the equations in this Appendix, then the same relationships exist between T_b^*, q^*, and $(Nu)_{am}$ with solidification as without solidification.

BIBLIOGRAPHY

Literature Cited

1. M. Jakob, Heat Transfer, Volume I, John Wiley and Sons, Inc., New York, 1958, pp. 451-464.

2. W. M. Kays, "Numerical Solutions for Laminar-Flow Heat Transfer in Circular Tubes," Transactions of the American Society of Mechanical Engineers, Vol. 77, 1955, pp. 1265-1274.

3. P. J. Schneider, "Effect of Axial Fluid Conduction on Heat Transfer in the Entrance Regions of Parallel Plates and Tubes," Trans. ASME, Vol.79, 1957, pp. 765-773.

4. S. N. Singh, "Heat Transfer by Laminar Flow in a Cylindrical Tube," Applied Scientific Research, Vol. A7, 1958, pp. 325-340.

5. J. R. Sellers, M. Tribus, and J. S. Klein, "Heat Transfer in Laminar Flow in a Round Tube or Flat Conduit - The Graetz Problem Extended," Trans. ASME, Vol. 78, 1956, pp. 441-448.

6. J. Schenk and J. M. Dumore, "Heat Transfer in Laminar Flow Through Cylindrical Tubes," Applied Scientific Research, Vol. A4, 1954, pp. 39-51.

7. H. C. Brinkman, "Heat Effects in Capillary Flow I," Applied Scientific Research, Vol. A2, 1951, pp. 120-124.

8. R. G. Deissler, "Analytical Investigation of Fully Developed Laminar Flow in Tubes with Heat Transfer with Fluid Properties Variable Along the Radius," NACA TN 2410, July, 1951.

9. K.-T. Yang, "Laminar Forced Convection of Liquids in Tubes with Variable Viscosity," Journal of Heat Transfer, Trans. ASME, Vol. 84, Series C, November, 1962, pp. 353-362.

10. E. M. Sparrow and R. Siegel, "Thermal Entrance Region of a Circular Tube Under Transient Heating Conditions," Proceedings of the Third U. S. National Congress of Applied Mechanics, 1958, pp. 817-826.

11. W. H. McAdams, Heat Transmission, 3rd ed., McGraw-Hill Book Company, Inc., New York, 1954, pp. 202-250.

12. J. G. Knudsen and D. L. Katz, Fluid Dynamics and Heat Transfer, McGraw-Hill Book Company, Inc., New York, 1958, pp. 361-390.

13. T. W. Jackson, J. M. Spurlock, and K. R. Purdy, "Combined Free and Forced Convection in a Constant Temperature Horizontal Tube," American Institute of Chemical Engineers Journal, Vol. 7, No. 1, 1961, pp. 38-41.

14. D. R. Oliver, "The Effect of Natural Convection on Viscous-Flow Heat Transfer in Horizontal Tubes," Chemical Engineering Science, Vol. 17, 1962, pp. 335-350.

15. H. S. Carslaw and J. C. Jaeger, Conduction of Heat in Solids, 2nd ed., Clarendon Press, Oxford, 1959, pp. 282-296.

16. G. Poots, "An Approximate Treatment of a Heat Conduction Problem Involving a Two-Dimensional Solidification Front," International Journal of Heat and Mass Transfer, Vol. 5, 1962, pp. 339-348.

17. A. Tkachev, "An Approximate Theoretical Solution of the Problem of Convective Heat Exchange in Fusion and Freezing," (in Russian), Kolodilnaya Tekhnika, No. 2, 1956, pp. 50-54; Applied Mechanics Reviews, Vol. 12, No. 3, 1959, Review 1519.

18. G. Horvay, "Freezing of a Growing Liquid Column," Journal of Heat Transfer, Trans. ASME, Vol. 82, Series C, February, 1960, pp. 37-47.

19. H. Bueckner and G. Horvay, "Heat-Transfer Coefficient of Inviscid Fluid Freezing Onto a Moving Heat Sink," Journal of Heat Transfer, Trans. ASME, Vol. 85, Series C, August, 1963, pp. 246-260.

20. C. A. Whitehurst, "Heat and Mass Transfer by Free Convection from Humid Air to a Metal Plate under Frosting Conditions," American Society of Heating, Refrigeration, and Air Conditioning Engineers Journal, Vol. 4, No. 5, 1962, pp. 58-69.

21. W. W. Brush, "Freezing of Water in Subaqueous Mains Laid in Salt Water and in Mains and Services Laid on land," Journal of the American Water Works Association, Vol. 3, 1916, pp. 962-980.

22. M. M. Chen and W. Rohsenow, "Heat, Mass, and Momentum Transfer Inside Frosted Tubes - Experiment and Theory," ASME Paper No. 63-HT-43.

23. H. G. Hirschberg, "Freezing of Piping Systems," (in German), Kaltetechnik, Vol. 14, No. 10, 1962, pp. 314-321.

24. A. I. Veynik, Theory of Special Casting Methods, The American Society of Mechanical Engineers, New York, 1954, pp. 1-145.

25. N. E. Dorsey, Properties of Ordinary Water-Substance, Reinhold Publishing Corporation, New York, 1940.

Other References

26. Agrawal, H. C., "A Variational Method for Combined Free and Forced Convection in Channels," International Journal of Heat and Mass Transfer, Vol. 5, 1962, pp. 439-444.

27. Belinfante, D. C., "On Viscous Flow in a Pipe with Constrictions," Proceedings of the Cambridge Philosophical Society, Vol. 58, No. 2, 1962, pp. 405-416.

28. Campbell, W. D. and J. C. Slattery, "Flow in the Entrance of a Tube," Journal of Basic Engineering, Trans. ASME, Vol. 85, Series D, March, 1963, pp. 41-46.

29. Horvay, G., "The Dip-Forming Process," ASME Paper No. 64-HT-3.

30. Kubaugh, B. F., "A Development in the Manufacture of Ice," Mechanical Engineering, Vol. 63, 1941, pp. 875-878.

31. Langlois, W. E., "Creeping Viscous Flow Through a Two-Dimensional Channel of Varying Gap," Proceedings of the Third U. S. National Congress of Applied Mechanics, 1958, pp. 777-783.

32. London, A. L. and R. A. Seban, "Rate of Ice Formation," Trans. ASME, Vol. 65, 1943, pp. 771-778.

33. Maslen, S. H., "On Fully Developed Channel Flows: Some Solutions and Limitations, and Effects of Compressibility, Variable Properties, and Body Forces," NACA TN 4319, September, 1958.

34. Millsaps, K. and K. Pohlhausen, "Thermal Distributions in Jeffrey-Hamel Flows Between Nonparallel Plane Walls," Journal of the Aeronautical Sciences, Vol. 20, March, 1953, pp. 187-196.

35. Morgan, G. W., "On the Steady Laminar Flow of a Viscous, Incompressible Fluid in an Elastic Tube," Bulletin of Mathematical Biophysics, Vol. 14, No. 19, 1952.

36. Narasimhan, M. N. L., "On the Steady Laminar Flow of a Viscous Liquid Through an Elastic Tube with Constant Temperature Gradient," Proceedings of the Second Congress of Theoretical Applied Mechanics, New Delhi, India; Indian Society of Theoretical Applied Mechanics, Indian Institute of Technology, 1956, pp. 153-164.

37. Poots, G., "On the Application of Integral-Methods to the Solution of Problems Involving the Solidification of Liquids Initially at the Fusion Temperature," International Journal of Heat and Mass Transfer, Vol. 5, 1962, pp. 525-531.

38. Prados, J. W. and F. N. Peebles, "Two-Dimensional Laminar-Flow Analysis Utilizing a Doubly Refracting Liquid," A.I.Ch.E. Journal, Vol. 5, No. 2, 1959, pp. 225-234.

39. Sparrow, E. M. and R. Siegel, "Application of Variational Methods to the Thermal Entrance Region of Ducts," International Journal of Heat and Mass Transfer, Vol. 1, 1960, pp. 161-172.

40. Tirskii, G. A., "An Exact Solution of the Energy Equation in a Particular Case of the Motion of a Viscous Incompressible Fluid," Applied Mathematics and Mechanics, Vol. 22, No. 4, 1958, pp. 777-786.

VITA

Ronald D. Zerkle was born on November 3, 1937, in Springfield, Ohio. There he attended elementary and secondary schools, graduating from Northeastern High School in 1955.

He entered the University of Cincinnati in 1955 and received a degree in Mechanical Engineering in 1960. While at the University of Cincinnati he participated in the co-operative program, and thereby gained two years of industrial experience at the International Harvester Company in Springfield, Ohio.

In 1960 he entered the Graduate School of Northwestern University and received the degree Master of Science in Mechanical Engineering in 1962. While at Northwestern University, he received support from a Walter P. Murphy fellowship.

During the summer of 1961 he was employed as a staff engineer in the Chemistry Division of the Argonne National Laboratory, and during the summer of 1962 he was employed as a research engineer at the Borg Warner Research Center in Des Plaines, Illinois.

In the fall of 1962 he entered the Georgia Institute of Technology to work toward the Doctor of Philosophy in Mechanical Engineering. Since then he has been a graduate teaching assistant and has received support from a Ford Foundation fellowship.

He is a student member of the American Society of Mechanical Engineers, and a member of the Societies of Pi Tau Sigma, Tau Beta Pi, and Sigma Xi.

In September, 1961, he married the former Sandra S. Souder, and they presently have two children, Mary Lisa and David Karl.